ELSEVIER

Journal of Fluids and Structures 25 (2009) 479–505

JOURNAL OF FLUIDS AND STRUCTURES

www.elsevier.com/locate/jfs

Vortex shedding from two finite circular cylinders in a staggered configuration

H. Li, D. Sumner*

Department of Mechanical Engineering, University of Saskatchewan, 57 Campus Drive, Saskatoon, Saskatchewan, Canada S7N 5A9

Received 6 June 2008; accepted 4 November 2008
Available online 5 March 2009

Abstract

Wind tunnel experiments were conducted to measure the vortex shedding frequencies for two circular cylinders of finite height arranged in a staggered configuration. The cylinders were mounted normal to a ground plane and were partially immersed in a flat-plate turbulent boundary layer. The Reynolds number based on the cylinder diameter was $\mathrm{Re}_D = 2.4 \times 10^4$, the cylinder aspect ratio was $\mathrm{AR} = 9$, the boundary layer thickness relative to the cylinder height was $\delta/H = 0.4$, the centre-to-centre pitch ratio was varied from $P/D = 1.125$ to 5, and the incidence angle was incremented in small steps from $\alpha = 0^\circ$ to 90°. The Strouhal numbers were obtained behind the upstream and downstream cylinders using hot-wire anemometry. From the behaviour of the Strouhal number data obtained at the mid-height position, the staggered configuration could be broadly classified by the pitch ratio as closely spaced ($P/D < 1.5$), moderately spaced ($1.5 \leqslant P/D \leqslant 3$), or widely spaced ($P/D > 3$). The closely spaced staggered finite cylinders were characterized by the same Strouhal number measured behind both cylinders, an indication of single bluff-body behaviour. Moderately spaced staggered finite cylinders were characterized by two Strouhal numbers at most incidence angles. Widely spaced staggered cylinders were characterized by a single Strouhal number for both cylinders, indicative of synchronized vortex shedding from both cylinders at all incidence angles. For selected staggered configurations representative of closely spaced, moderately spaced, or widely spaced behaviour, Strouhal number measurements were also made along the vertical lengths of the cylinders, from the ground plane to the free end. The power spectra showed that for certain cylinder arrangements, because of the influences of the cylinder–wall junction and free-end flow fields, the Strouhal numbers and flow patterns change along the cylinder.

Keywords: Bluff-body aerodynamics; Finite circular cylinder; Multiple cylinders; Staggered cylinders; Vortex shedding; Wake interference

1. Introduction

As one of the most fundamental research topics of bluff-body aerodynamics, the flow around the circular cylinder has been widely investigated due to the common occurrence of cylinder-like structures in engineering applications, such as buildings, power transmission lines, chimney stacks, offshore structures, and the pipes in a heat exchanger. In many of

*Corresponding author. Tel.: +1 306 966 5537; fax: +1 306 966 5427.
E-mail address: david.sumner@usask.ca (D. Sumner).

0889-9746/$ - see front matter © 2008 Elsevier Ltd. All rights reserved.
doi:10.1016/j.jfluidstructs.2008.11.001

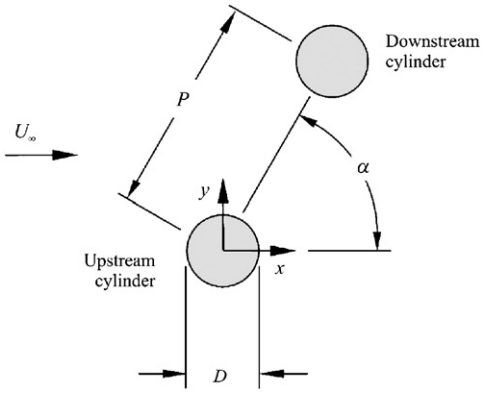

Fig. 1. Staggered configuration of two infinite circular cylinders of equal diameter in uniform steady cross-flow, where U_∞ is the freestream velocity, x is the streamwise coordinate, y is the cross-stream coordinate, P is the centre-to-centre pitch (or spacing), and α is the incidence angle.

these engineering applications, Kármán vortex shedding may be responsible for problems with flow-induced vibration and noise.

In some engineering fluid flow applications, cylindrical structures appear in groups. The staggered configuration is the most general arrangement of two circular cylinders in cross-flow (Fig. 1). The geometry of the staggered pair of cylinders, each of the same diameter, D, immersed in steady uniform cross-flow of velocity U_∞, is set by the centre-to-centre pitch (or spacing) between the cylinders, P, and the angle of incidence, α (Fig. 1). Studies of the flow around two staggered "infinite" circular cylinders have revealed complex interactions between the shear layers, wakes, and Kármán vortex streets of the individual cylinders. These lead to the appearance of a wide range of flow patterns (Fig. 2), which are functions of the dimensionless centre-to-centre pitch ratio, P/D, and α (Zdravkovich and Pridden, 1977; Gu and Sun, 1999; Sumner et al., 2000, 2005; Akbari and Price, 2005).

The vortex shedding frequency for a circular cylinder, f, is represented in dimensionless form as the Strouhal number, St ($=fD/U_\infty$). For many staggered configurations of two "infinite" circular cylinders, two Strouhal numbers are measured (Kiya et al., 1980; Sumner et al., 2000, 2005). In other cases, an absence of reliable Strouhal number has been reported for specific combinations of P/D and α, suggesting a weakened or absent vortex shedding activity (Sumner and Richards, 2003; Sumner et al., 2005). Within the subcritical Reynolds number regime (the Reynolds number, $\mathrm{Re}_D = U_\infty D/\nu$, where ν is the kinematic viscosity), the general behaviour of St depends on whether the cylinders are closely spaced ($P/D<1.5$), moderately spaced ($1.5\leqslant P/D\leqslant 2.5$) or widely spaced ($P/D>2.5$) (Sumner et al., 2005). For closely spaced staggered infinite circular cylinders, the same Strouhal number is measured behind the upstream and downstream cylinders (i.e., when measuring in the free shear layer originating from the upstream cylinder, or when measuring in the free shear layer originating from the downstream cylinder, the same Strouhal number value is measured), which indicates that a single vortex shedding process is present. The detection of a single Strouhal number is consistent with the closely spaced cylinders behaving as a single bluff body. For moderately spaced staggered infinite cylinders, two distinct Strouhal numbers are measured for a wide range of α. Based on the measurement location, the higher Strouhal number broadly corresponds to vortex shedding from the upstream cylinder and the lower Strouhal number broadly corresponds to vortex shedding from the downstream cylinder. For widely spaced staggered infinite cylinders, the same Strouhal number is measured behind both cylinders for most α. Both cylinders are seen to undergo vortex shedding at the same frequency. This Strouhal number remains close to that of a single, isolated circular cylinder indicating the reduced effects of interference between the cylinders (Sumner et al., 2005).

Many of the cylinder-like structures encountered in engineering applications are better approximated as "finite" circular cylinders (e.g., Taniguchi et al., 1981; Sakamoto and Arie, 1983; Sakamoto and Oiwake, 1984; Uematsu et al., 1990; Okamoto and Sunabashiri, 1992; Tanaka and Murata, 1999; Park and Lee, 2000; Sumner et al., 2004; Adaramola et al., 2006) as opposed to "infinite" circular cylinders. Fig. 3 shows a circular cylinder of finite height mounted normal to a ground plane and partially immersed in a flat-plate boundary layer, where $U(z)$ is the incoming flow velocity profile, z is the wall-normal coordinate, H is the height of the cylinder, and δ is the thickness of the boundary layer. The essential distinction between the flow patterns of the infinite circular cylinder and the finite circular cylinder is that the flow field around the infinite cylinder can generally be treated as two-dimensional while the flow structure for the finite cylinder is strongly three-dimensional due to the existence of its base (cylinder–wall junction) and free end. The free end causes the formation of a pair of counter-rotating vortices, which induces strong "downwash" flow from the top of the

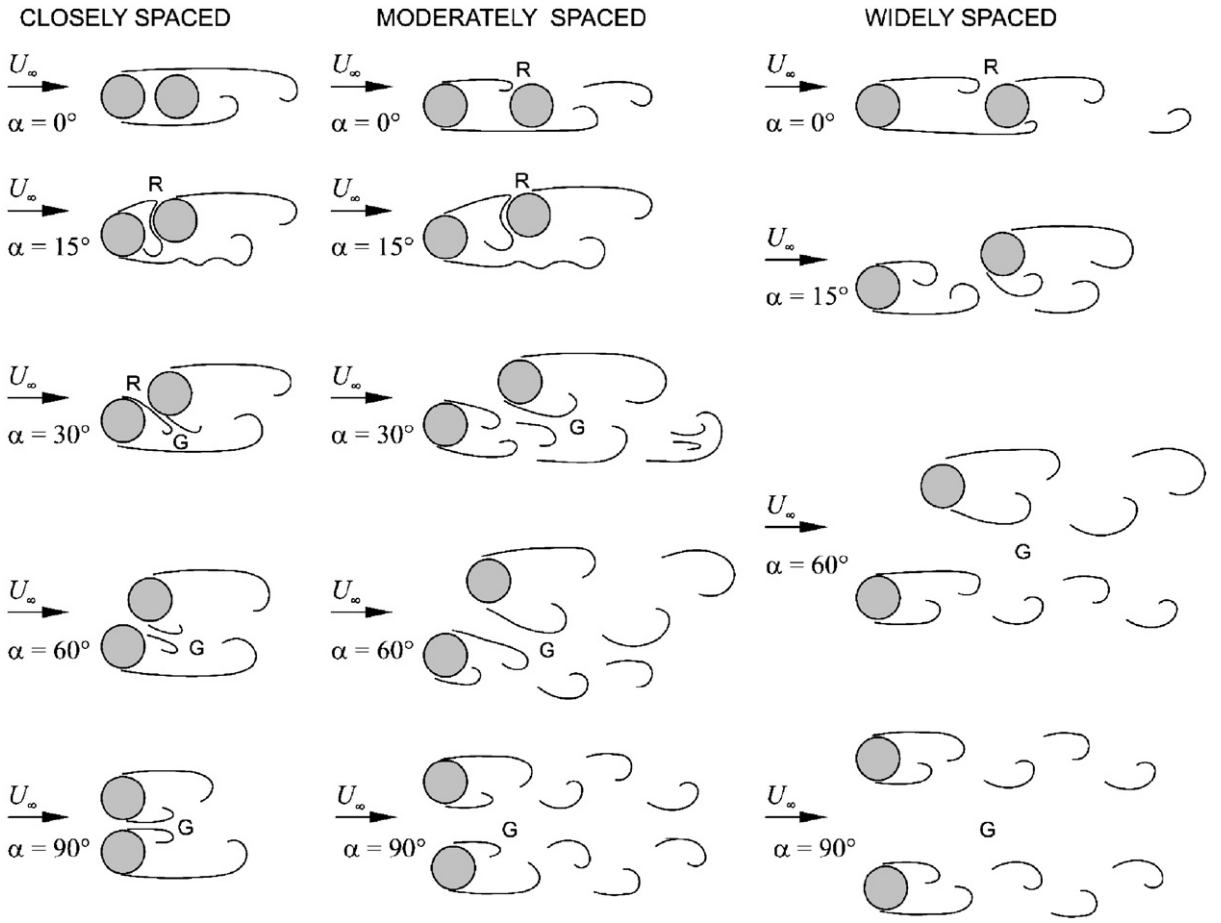

Fig. 2. Overview of flow patterns for two staggered *infinite* circular cylinders of equal diameter in steady cross-flow, based on Sumner et al. (2000, 2005). R = reattachment; G = gap.

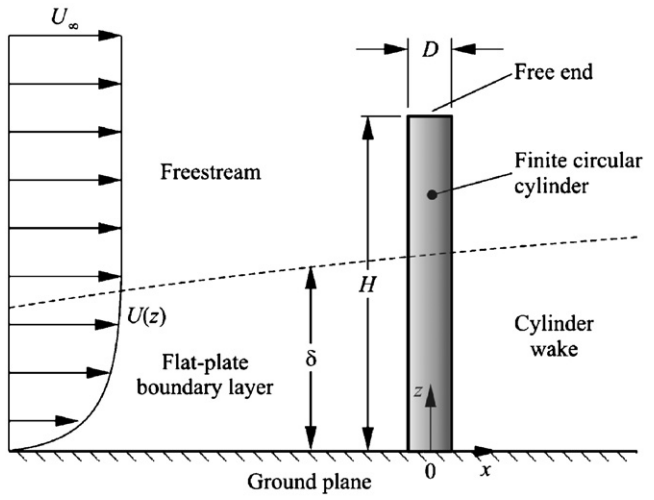

Fig. 3. Circular cylinder of finite height mounted normal to a ground plane and partially immersed in a flat-plate boundary layer.

finite cylinder. Within the near-wake and intermediate wake, this "downwash" flow interacts with the regular Kármán vortex shedding from the two sides of the cylinder, resulting in weakened or suppressed vortex shedding and a three-dimensional flow structure near the free end of the cylinder. In addition, the regular vortex shedding around the base of the finite circular cylinder is affected by the flat-plate boundary layer and the steady horseshoe vortex structure generated at the cylinder–wall junction. These two factors contribute to the highly three-dimensional and complicated flow behaviour behind the finite cylinder.

The flow field of the finite circular cylinder is strongly influenced by the cylinder's aspect ratio, $AR = H/D$, and the thickness of the boundary layer developed on the wall relative to the cylinder height and diameter, i.e. the ratios δ/H and δ/D. For higher aspect ratios, the Strouhal number may vary in a cellular fashion along the cylinder height, each cell having a different frequency, with shedding being suppressed near the free end and near the cylinder–wall junction. The cellular structure disappears at lower aspect ratios, becoming a single cell of uniform St along the entire vertical length of the cylinder (Uematsu et al., 1990; Okamoto and Sunabashiri, 1992), particularly when δ/H is large (Sakamoto and Oiwake, 1984). For smaller aspect ratios, however, the flow around the free end may completely suppress antisymmetric Kármán vortex shedding from the cylinder, from the base to the tip. The critical aspect ratio below which antisymmetric vortex shedding is suppressed varies between the different studies in the literature, from $AR = 1$ to 7. At and below the critical aspect ratio, antisymmetric Kármán vortex shedding may be replaced with symmetric arch vortex shedding at a definite frequency (Taniguchi et al., 1981; Sakamoto and Arie, 1983; Okamoto and Sunabashiri, 1992; Tanaka and Murata, 1999).

When two finite circular cylinders are arranged in a staggered configuration, the interaction between the downwash flows from the two cylinders, along with the strong flow interference happening at the bases of the two cylinders, makes the flow pattern even more complex and challenging to investigate. Owing to the complexities in the flow behaviour behind the finite circular cylinder, there are a relatively limited number of investigations on the flow around *groups* of two finite circular cylinders (e.g., Taniguchi et al., 1982; Luo et al., 1996; Park and Lee, 2003). Most of the previous research work on the flow around two staggered finite circular cylinders has been focused on measurements of the mean pressure distributions and aerodynamic forces. Comparably less attention has been directed towards vortex shedding from two staggered finite circular cylinders, and this has motivated the present study.

2. Literature review

One of the earlier studies on the flow around groups of two finite circular cylinders mounted normal to a plane wall, by Zdravkovich (1980), measured the circumferential mean pressure distributions (and mean lift and drag forces) along the vertical axes of two staggered finite circular cylinders of $AR = 4.6$ at $Re_D = 2 \times 10^5$, with $P/D = 1.325$ and $\alpha = 15^\circ$, 45° and 90°. There was no appreciable boundary layer on the plane wall, i.e. $\delta/H \approx 0$. For the staggered configurations of $\alpha = 15^\circ$ and 45°, the strongest effects of the free end and base regions were experienced by the downstream cylinder, and the strength of the gap flow was found to decrease closer to the free end. For the side-by-side configuration (corresponding to $\alpha = 90^\circ$), the bistable biased flow pattern existed, similar to what is found for two side-by-side infinite circular cylinders (Sumner et al., 1999).

Sarode et al. (1981) presented some data for the mean drag force acting on the downstream cylinder for two tandem (corresponding to $\alpha = 0^\circ$) finite circular cylinders of $AR = 4.09$ at $Re_D = 2.2 \times 10^4$, with $P/D = 1$–8. The cylinders were immersed in a simulated atmospheric boundary layer. Their limited results showed that the interference effects were similar to those reported for two tandem infinite cylinders.

In a more comprehensive study, Taniguchi et al. (1982) examined the interference between two staggered finite circular cylinders of $AR = 3$ at $Re_D = 1.55 \times 10^4$, with $P/D = 1.2$–4 and $\alpha = 0$–90°. The boundary layer thickness at the location of the cylinder was $\delta/H = 0.4$. They presented measurements of the mean pressure distributions on the cylinders' surfaces at different locations above the ground plane, from which they obtained the mean drag and lift force coefficients. The pressure distributions showed that the flow patterns could change along the cylinders, in particular for the downstream cylinder, due to the influence of the tip flow from the upstream cylinder. According to the behaviour of the mean drag and lift force coefficients, the flow pattern was broadly divided into three regimes based on incidence angle: $0^\circ \leqslant \alpha \leqslant 30^\circ$, $30^\circ \leqslant \alpha \leqslant 120^\circ$, and $120^\circ \leqslant \alpha \leqslant 180^\circ$ (where $\alpha > 90^\circ$ corresponds to the outer cylinder becoming an upstream cylinder; see Fig. 1). Graphs of iso-drag and iso-lift coefficient contour lines, as a function of cylinder position, were qualitatively similar to the infinite-cylinder results of Zdravkovich and Pridden (1977).

Kareem et al. (1998) investigated the interference effects for two finite circular cylinders of $AR = 10$ in cross-flow by measuring the mean and r.m.s aerodynamic forces on the upstream and downstream cylinders. The spectra of the r.m.s. lift coefficient data yielded some information on the vortex shedding frequencies. The cylinders were immersed in a

simulated atmospheric boundary layer at $Re_D = 2.7 \times 10^4$, and arranged in moderately and widely spaced staggered configurations of $P/D = 2$–7 at six different incidence angles. In general, the strongest interference effects were found for the downstream cylinder. Vortex impingement was responsible for elevated r.m.s. lift and drag coefficients on the downstream cylinder. They identified configurations corresponding to minimum mean drag, similar to what has been reported for two infinite cylinders (Zdravkovich and Pridden, 1977; Sumner et al., 2005). The force spectra showed weakened vortex shedding from the downstream cylinder, for $P/D \leqslant 3$, compared to the single, isolated finite circular cylinder.

Luo et al. (1996) studied the flow around two tandem finite circular cylinders by measuring the circumferential mean pressure distributions along the cylinders. Cylinders with different aspect ratios, of AR = 4, 6 and 8, were arranged in tandem at pitch ratios of $P/D = 1$ (corresponding to the cylinders in contact), 1.64, 3 and 5. The experiments were conducted at $Re_D = 3.33 \times 10^4$ and there was no appreciable boundary layer on the plane wall, i.e. $\delta/H \approx 0$. For the cylinders with AR = 8, where the most interesting results occurred, the downstream cylinder showed the most variation in the mean pressure distribution along the cylinder's vertical length, due to the influence of the tip vortices emanating from the upstream cylinder impinging upon the downstream cylinder. Although the flow patterns were generally similar to the case of two tandem infinite circular cylinders, they reported, similar to Taniguchi et al. (1982), that the flow pattern could vary along the vertical lengths of the finite cylinders. For example, for $P/D = 1.64$, flow from the upstream cylinder reattached onto the downstream cylinder along nearly the entire vertical length. However, for $P/D = 3$ and 5, vortex shedding occurred from both cylinders (''co-shedding'') on the upper sections of the cylinders while reattached flow occurred over the middle and lower sections of the cylinders.

Park and Lee (2003) studied the flow around two finite circular cylinders of AR = 6 arranged in the side-by-side configuration at $Re_D = 2 \times 10^4$, using flow visualisation, hot-wire anemometry, and surface static pressure measurements. The cylinders were immersed in a simulated atmospheric boundary layer. They investigated closely spaced and moderately spaced configurations of $P/D = 1$, 1.25, 1.5, 1.75 and 2. Similar to Zdravkovich (1980), they showed the existence of the bistable biased flow pattern for $P/D = 1.25$–1.75. Mean pressure distributions along the cylinder for $P/D = 1.5$ showed a gradual increase in the mean base pressure when moving further away from the free end. For $P/D = 2$, each cylinder had a pair of tip vortex structures, and Kármán vortex shedding was in-phase (i.e., symmetric on either side of the gap between the cylinders) on the upper portion of the cylinder near the free end. Measurements of the vortex shedding frequencies at the mid-height ($z/H = 0.5$) position showed that the strength of the vortex shedding peak in the power spectrum varied with P/D.

Liu and Cui (2006) simulated the flow past two side-by-side finite circular cylinders of AR = 10 at $Re_D = 200$ using the lattice-Boltzmann method; no information was provided on whether a boundary layer was modeled on the ground plane. Their results showed the existence of the biased flow pattern for $P/D = 1.2$, 1.5 and 2. Their instantaneous vorticity contours suggested that the biased flow pattern disappears near the free end, due to the influence of the flow about the free end and the suppression or weakening of Kármán vortex shedding in this region.

Krönke and Sockel (2007) measured the mean, r.m.s., and extreme values of the aerodynamic forces experienced by two staggered finite circular cylinders of AR = 8 at $Re_D = 4 \times 10^4$, with $P/D = 1.5$, 2, 3 and 5 and $\alpha = 0$–30°. Only limited results were presented, which focused mainly on the effects of different simulated atmospheric boundary layers. The authors showed that elevated freestream turbulence intensity reduced the interference effects between the cylinders. They also observed critical values of incidence angle, which corresponded to local minimum values of the mean and extreme values of the aerodynamic forces, similar to what has been well-documented for two staggered infinite circular cylinders (e.g., Zdravkovich and Pridden, 1977; Sumner et al., 2005).

Palau-Salvador et al. (2007) used large-eddy simulation (LES) to model the flow around two tandem finite circular cylinders of AR = 2.5 at $Re_D = 1500$ with $P/D = 2$. There was no boundary layer on the ground plane, i.e. $\delta/H \approx 0$. The results showed that at this pitch ratio, the flow structure had the characteristics of the reattachment flow pattern with no vortex shedding in the gap between the two cylinders; this is similar to the case for two infinite circular cylinders in tandem. The tip vortices from the upstream cylinder entered the gap between the cylinders and impinged upon the downstream cylinder. Consequently, the separation lines on the surface of the downstream cylinder were much different than those observed on the surface of the upstream cylinder and those found on the surface of a single, isolated finite circular cylinder.

From a review of the literature, it is seen that relatively few studies of two finite circular cylinders in cross-flow have extensively considered the vortex shedding behaviour. Although Rooney et al. (1995) studied the vortex shedding from a staggered arrangement of two finite circular cylinders, their experiments involved two cylinders of *different* aspect ratio (i.e., the cylinders were not identical); their study was more focused on the influence of the different aspect ratios rather than on the effect of pitch ratio and incidence angle. In the present study, therefore, low-speed wind tunnel experiments were conducted to examine the characteristics of the vortex shedding frequencies (Strouhal numbers) for two staggered finite circular cylinders of AR = 9, for different combinations of P/D and α, at $Re_D = 2.4 \times 10^4$.

The cylinders were mounted normal to a ground plane and were partially immersed in a flat-plate turbulent boundary layer, with $\delta/H = 0.4$. The finite-cylinder results are compared to the Strouhal number data from Sumner et al. (2005) for two staggered *infinite* circular cylinders.

3. Experimental approach

The experiments were conducted in a low-speed, closed-return wind tunnel with a test-section of 0.91 m (height) × 1.13 m (width) × 1.96 m (length). The longitudinal freestream turbulence intensity was less than 0.6% and the velocity non-uniformity outside the test-section wall boundary layers was less than 0.5%. The experiments were conducted at a freestream velocity of $U_\infty = 20$ m/s.

The experimental set-up is shown schematically in Fig. 4. Two identical circular cylinders of $H = 171.45$ mm, $D = 19.1$ mm and AR = 9, were arranged in staggered configurations in the test-section. The cylinders were made of aluminium and had a smooth finish. The experiments were conducted at a cylinder Reynolds number of $\mathrm{Re}_D = 2.4 \times 10^4$.

A smooth, flat ground plane was installed near the test-section floor. A boundary layer trip was positioned downstream of the leading edge of the ground plane. At the position of the finite circular cylinders, the turbulent flat-plate boundary layer developing on the ground plane was 68 mm thick. The ratio of the boundary thickness, δ, to the height of the cylinder was $\delta/H = 0.4$.

The set-up for arranging the cylinders in different staggered configurations was similar to that adopted by Sumner and Richards (2003) and Sumner et al. (2005). The first cylinder, known as the central cylinder, was mounted vertically from a six-component force balance located outside and below the wind tunnel test-section. This cylinder was centrally located in the test-section. The second cylinder, known as the outer cylinder, was mounted onto a turntable embedded in the ground plane. The turntable was driven by a timing belt, stepping motor and microstep driver. By rotating the outer cylinder on the turntable through 180°, the fixed central cylinder could represent either an upstream or downstream cylinder for staggered configurations with incidence angles from $\alpha = 0°$ to 90°. Pitch ratios of $P/D = 1.125$, 1.25, 1.5, 2, 2.5, 3, 4 and 5 were used in the experiments; a set of mounting holes in the turntable allowed the outer cylinder to be located at different positions to give the above pitch ratios.

The experimental data were acquired with a Pentium 4 computer running Windows XP Professional, a National Instruments PCI-6031E 16-bit multifunction board and LabVIEW software. Reference flow conditions were measured

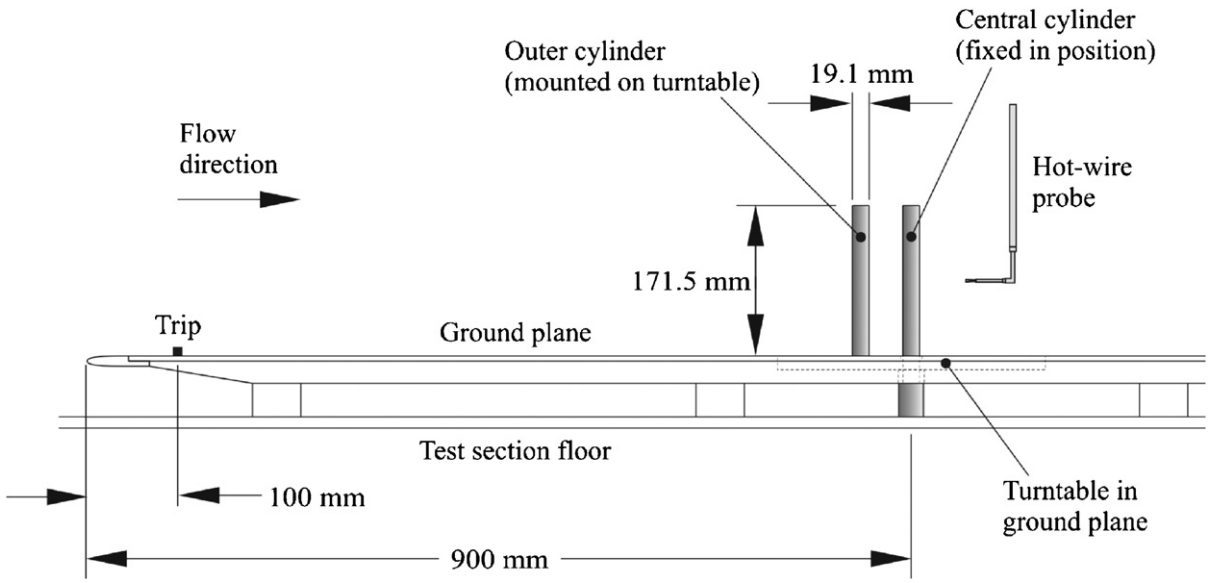

Fig. 4. Experimental set-up in the wind tunnel for the two staggered finite circular cylinders mounted normal to the ground plane (shown for $P/D = 3$, $\alpha = 0°$, where the outer cylinder is positioned on the turntable to represent an upstream cylinder). The hot-wire probe is shown positioned at the mid-height of the cylinders at a streamwise distance of $x = 3D$ behind the central cylinder.

with a Pitot-static probe (United Sensor, 3.2-mm diameter) and Datametrics Barocell absolute and differential pressure transducers. Vortex shedding frequencies were measured with a TSI 1210-T1.5 single-component hot-wire probe, a TSI IFA-100 anemometer, and the signal analysis (FFT) virtual instruments in the LabVIEW software. Using a three-axis computer-controlled traversing system, the probe was located behind the central cylinder at a fixed streamwise and cross-stream position of $x/D = 3$ and $y/D = 1$, with the wall-normal position (z/H) allowed to vary to measure the vortex shedding frequencies along the vertical lengths of the cylinders. In some cases where no Strouhal numbers could be found, the streamwise and cross-stream positions of the probe were changed to ensure the reliability and repeatability of the power spectra. The uncertainty in the Strouhal number was estimated to be $\mathrm{St} \pm 0.003$.

4. Results and discussion

Strouhal number measurements were first made along the vertical length of a single, isolated finite circular cylinder (i.e., behind the central cylinder with the outer cylinder removed). A Strouhal number of $\mathrm{St} = 0.160$ was measured at the mid-height position ($z/H = 0.5$). The power spectra measured along the cylinder are shown in Fig. 5, where it can be seen that the shape and strength of the vortex shedding peak varies with z/H. The peaks are weaker and more broad-banded near the free end and the base of the cylinder, which is consistent with earlier single-cylinder studies (e.g., Sumner et al., 2004). In addition, a second, weaker low-frequency peak is detected near the free end, corresponding to $\mathrm{St} = 0.067$–0.076. This low-frequency peak may represent a periodicity associated with the tip vortex structures and the separated flow from the free end (Kitigawa et al., 2002).

For the staggered cylinders, two main sets of experiments were performed. In the first set of experiments, the Strouhal numbers were measured at the mid-height position of the cylinders, i.e. the hot-wire probe was fixed at $z/H = 0.5$. Strouhal number data were collected for the upstream and downstream cylinders for each of the eight pitch ratios, using an incidence angle increment of 1° or 2° (depending on the region of interest), in order to cover the full range of incidence angle from $\alpha = 0^\circ$ to 90°. These results are reported in Section 4.1, where comparison is made to the infinite-cylinder results of Sumner et al. (2005). In the second set of experiments, Strouhal number measurements were made along the vertical lengths of the cylinders, i.e. where the wall-normal position of the hot-wire probe, z/H, was varied. These experiments were conducted for selected staggered configurations only, i.e. for specific combinations of P/D and α, in order to determine whether the Strouhal numbers change depending on their proximity to the ground plane and the free ends of the cylinders. The results from these experiments are reported in Section 4.2.

4.1. Strouhal number measurements at mid-height ($z/H = 0.5$)

For the measurements at the mid-height ($z/H = 0.5$) of the two staggered finite circular cylinders, the experimental data (Figs. 6–11) showed that the Strouhal number behaviour could be broadly classified according to pitch ratio, into closely spaced configurations ($P/D = 1.125$, 1.25), moderately spaced configurations ($P/D = 1.5$, 2, 2.5, 3) and widely spaced configurations ($P/D = 4$, 5). This was similar to what Sumner et al. (2005) found for two staggered infinite circular cylinders. However, for the finite cylinders, moderately spaced behaviour was found for a larger range of pitch ratio, up to $P/D = 3$ rather than $P/D = 2.5$. This result can be attributed to the longer vortex formation length and associated larger interference region for the finite circular cylinder compared to the infinite circular cylinder (Sumner et al., 2004).

4.1.1. Closely spaced staggered configurations ($P/D = 1.125$, 1.25)

Mid-height Strouhal number data for the closely spaced staggered configurations of $P/D = 1.125$, 1.25, plotted against incidence angle, are shown in Fig. 6. The behaviour of the finite-cylinder data is very similar to the infinite-cylinder data, except that the finite-cylinder Strouhal numbers are smaller than the infinite-cylinder Strouhal numbers. The downward shift of the finite-cylinder data points away from the infinite-cylinder data points is similar to the difference between the Strouhal numbers for single isolated finite ($\mathrm{St} = 0.160$) and infinite cylinders ($\mathrm{St} = 0.193$). For the single finite cylinder, downwash flow from the free end enters the near-wake, lengthens the vortex formation region and reduces the vortex shedding frequency (Park and Lee, 2000; Sumner et al., 2004).

In most cases, at a given combination of pitch ratio and incidence angle (Fig. 6), the same Strouhal number is measured behind the upstream and downstream cylinders, which indicates that at the mid-height position the finite cylinders are behaving as if they were a single bluff body with a single vortex shedding process (Sumner et al., 2000, 2005). A "critical incidence angle" of $\alpha \approx 10^\circ$ exists for both $P/D = 1.125$ and 1.25 (Fig. 6), where the Strouhal number

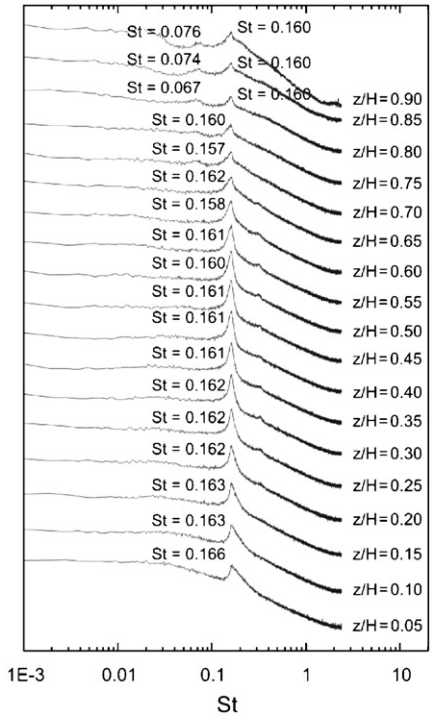

Fig. 5. Power spectra along the vertical length of a single finite circular cylinder, $Re_D = 2.4 \times 10^4$, AR = 9, $\delta/H = 0.4$. The hot-wire probe was positioned at $x/D = 3$ and $y/D = 1$. Each spectrum represents an average of 250 spectra. The vertical (logarithmic) scale of the graph is arbitrary, but the same scale is used for each spectrum.

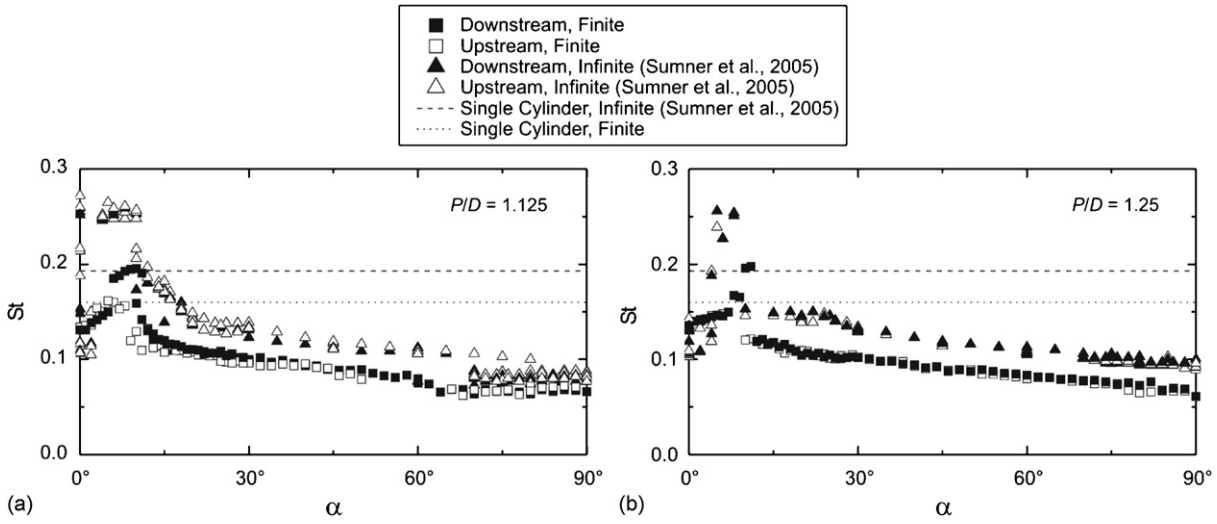

Fig. 6. Strouhal number data measured at mid-height ($z/H = 0.5$) for two closely spaced staggered finite circular cylinders: (a) $P/D = 1.125$; (b) $P/D = 1.25$. Open symbols: upstream cylinder; solid symbols: downstream cylinder; triangle symbols: infinite cylinders; square symbols: finite cylinders. For two staggered finite circular cylinders, $Re_D = 2.4 \times 10^4$, AR = 9, $\delta/H = 0.4$. For two staggered infinite circular cylinders, $Re_D = 3.2 \times 10^4$–7.3×10^4.

reaches a local maximum value.[1] Below the critical incidence angle, the finite-cylinder Strouhal number data have less scatter than the infinite-cylinder Strouhal number data.

When the incidence angles are greater than the critical value (Fig. 6), the Strouhal number is lower than that of a single finite circular cylinder and decreases gradually with increasing α. This result can be attributed to more of the approach flow entering the gap at higher α, resulting in a "base-bleed" flow pattern (Sumner et al., 2000). The base-bleed flow from the gap between the cylinders interacts with the two shear layers, resulting in an increase in the vortex formation length and the slow reduction in the Strouhal number. For $P/D = 1.125$ (Fig. 6(a)), the sharp discontinuity in the Strouhal number data at $\alpha \approx 70^\circ$ seen for two closely spaced infinite cylinders is absent. This sharp discontinuity is attributed to sudden changes in the base-bleed gap flow (Sumner et al., 2005). Instead, the Strouhal number of the finite cylinders smoothly shifts to a lower value at $\alpha \approx 60^\circ$ with increasing α. This suggests that the base-bleed flow may have less influence on the vortex shedding behaviour of the finite cylinders compared with the infinite cylinders, and the flow pattern changes more gradually for the finite cylinders when the base-bleed flow starts to penetrate the near-wake region.

The vortex shedding peaks behind the upstream cylinder and downstream cylinder are shown in the power spectra in Fig. 7. The peaks are strong and sharp when the incidence angles are lower than the critical incidence angle, and become weak and broad-banded as the near-wake region behind the two cylinders gets wider at higher α. Especially for $\alpha > 70^\circ$, where the base-bleed flow begins to occur and creates a broader near-wake region and a longer vortex formation length behind the two cylinders, the vortex shedding process is weakened and the peaks are very weak; a similar behaviour of the vortex shedding peaks at high α was also detected for the infinite-cylinder cases (Sumner et al., 2005). For $P/D = 1.125$ (Fig. 7(a)), there is no peak at $\alpha = 10^\circ$ and 12° (near the critical incidence angle), and two peaks are observed behind the upstream cylinder when the cylinders are in tandem ($\alpha = 0^\circ$) due to the transition of the flow pattern along the vertical length of the cylinder (this is discussed further in Section 4.2.1); this phenomenon is not seen from the results of two tandem *infinite* cylinders (Sumner et al., 2005). For $P/D = 1.25$ (Fig. 7(b)), no detectable peak is measured behind the upstream cylinder at $\alpha = 8^\circ$ (near the critical incidence angle).

4.1.2. *Moderately spaced configurations ($P/D = 1.5, 2, 2.5, 3$)*

Mid-height Strouhal number data for the moderately spaced staggered configurations of $P/D = 1.5$, 2, 2.5 and 3 are shown in Fig. 8. The behaviour of the Strouhal number data is distinct from that of the closely spaced cylinders discussed in the previous section.

When the two cylinders are nearly in tandem and the incidence angle is small, the same Strouhal number is measured behind both the upstream and downstream cylinders; this can be attributed to a shear layer reattachment (SLR) flow pattern (Sumner et al., 2000) occurring at the mid-height position, where the cylinders behave as if they were a single bluff body. This Strouhal number increases in magnitude as α approaches a critical incidence angle of $\alpha \approx 12^\circ$. This behaviour is similar to two staggered *infinite* cylinders, but there is less scatter in the St data for the *finite* cylinders.

At the critical incidence angle (Fig. 8), the Strouhal numbers from the upstream cylinder and downstream cylinder become distinct; unlike the infinite-cylinder case (Sumner et al., 2005), a peak value of Strouhal number is not detected at the critical incidence angle. For incidence angles larger than the critical value, a higher Strouhal number is measured behind the upstream cylinder and a lower Strouhal number is measured behind the downstream cylinder (for some configurations, both Strouhal numbers can be measured behind the downstream cylinder). This change in the St behaviour corresponds to a transition from the SLR flow pattern to either an induced separation (IS), vortex pairing and enveloping (VPE), vortex pairing, enveloping and splitting (VPSE), or synchronized vortex shedding (SVS) flow pattern (Sumner et al., 2000), with Kármán vortex shedding occurring separately and distinctly from both cylinders at the mid-height position. This behaviour is identical for the finite and infinite cylinders, and is the main characterizing feature of the moderately spaced configurations.

For $P/D = 1.5$ (Fig. 8(a)), the Strouhal number measured behind the upstream cylinder continues to increase when α is larger than the critical incidence angle. It obtains a maximum value at $\alpha \approx 45^\circ$ where $St = 0.47$ and then drops gradually to $St = 0.1$ as α reaches 90°. Similar behaviour happens for $P/D = 2$, 2.5 and 3 (Figs. 8(b)–(d), respectively). However, due to the two cylinders spaced further away, both the maximum value of the St, and the incidence angle

[1]For two staggered *infinite* circular cylinders at closely and moderately spaced staggered configurations, the critical incidence angle is where the mean drag force coefficient on the upstream cylinder reaches a local minimum value, the downstream cylinder experiences a maximum inward-directed mean lift force coefficient (known as the "inner lift peak") and a local minimum mean drag coefficient (Zdravkovich and Pridden, 1977; Sumner et al., 2005). In addition, the Strouhal number attains a local maximum value at the critical incidence angle (Sumner et al., 2005). Here, for the two *finite* circular cylinders in closely and moderately spaced staggered configurations, in the absence of any force measurements (this will be a subject for future research), the critical incidence angle is defined by the local maximum value of the Strouhal number.

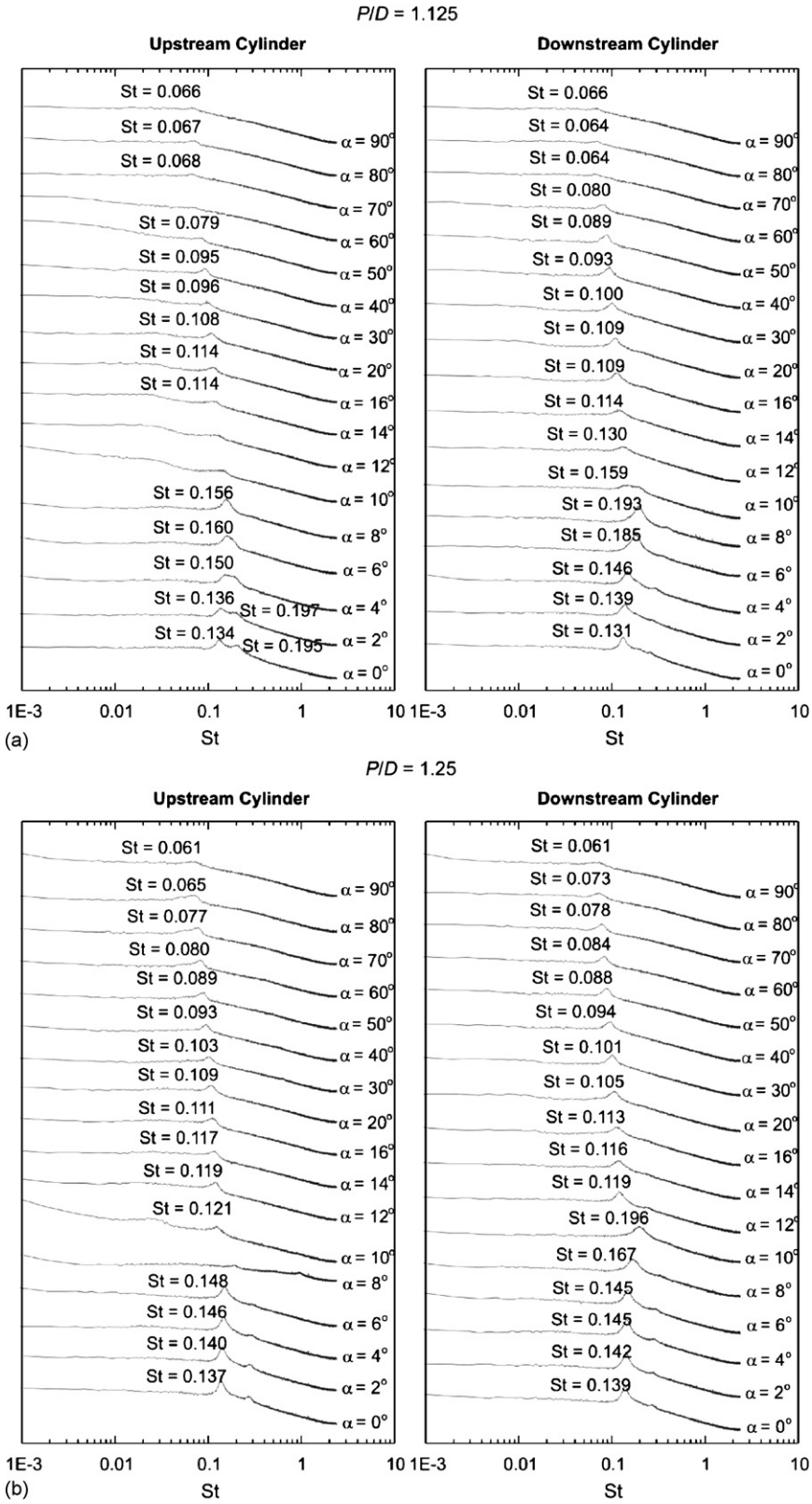

Fig. 7. Selected power spectra at mid-height ($z/H = 0.5$), as a function of incidence angle, for closely spaced staggered finite circular cylinders: (a) $P/D = 1.125$; (b) $P/D = 1.25$. Each spectrum represents an average of 250 spectra. The vertical (logarithmic) scale of the graphs is arbitrary, but the same scale is used for each spectrum.

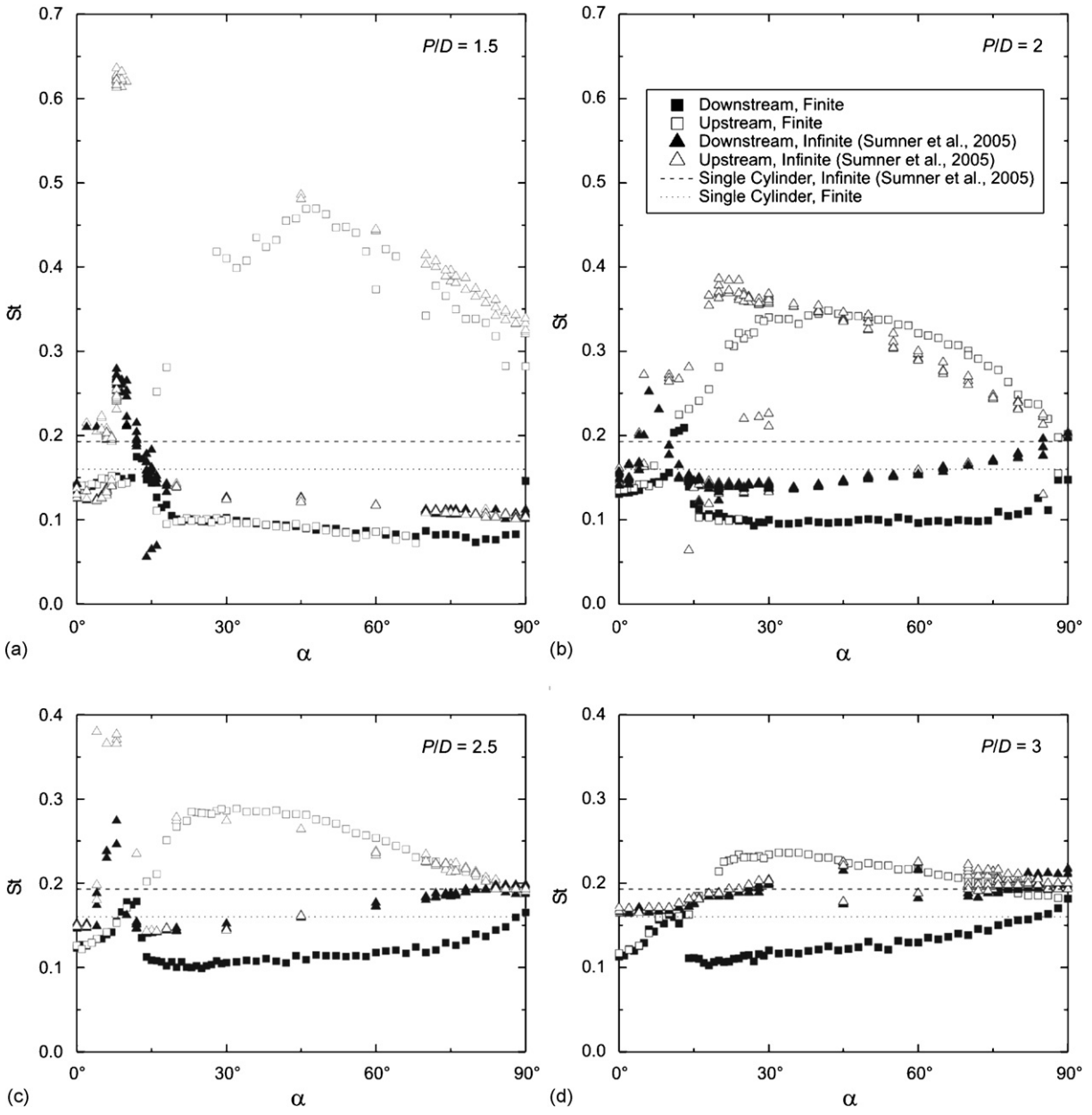

Fig. 8. Strouhal number data measured at mid-height ($z/H = 0.5$) for two moderately spaced staggered finite circular cylinders: (a) $P/D = 1.5$; (b) $P/D = 2$; (c) $P/D = 2.5$; (d) $P/D = 3$. Symbols as in Fig. 6.

where the maximum St is obtained, decrease. The St values measured from the upstream *finite* cylinder are close to those for the infinite-cylinder case, but the St values for the downstream *finite* cylinder are lower than the infinite-cylinder case. This result is consistent with some of the previous studies of two finite cylinders, which showed the strongest interference effects are experienced by the downstream cylinder (e.g., Zdravkovich, 1980; Luo et al., 1996; Kareem et al., 1998).

The power spectra for the two moderately spaced cylinders are shown in Fig. 9, where it can be seen that the higher of the two Strouhal numbers is measured behind the upstream cylinder and the lower of the two Strouhal numbers is measured behind the downstream cylinder. The vortex shedding peaks for the upstream cylinder tend to be stronger and sharper compared to those of the downstream cylinder, which are typically weaker and more broad-banded. For $P/D = 1.5$ (Fig. 9(a)) and $P/D = 2$ (Fig. 9(b)), both the high and low Strouhal number peaks can be found behind the

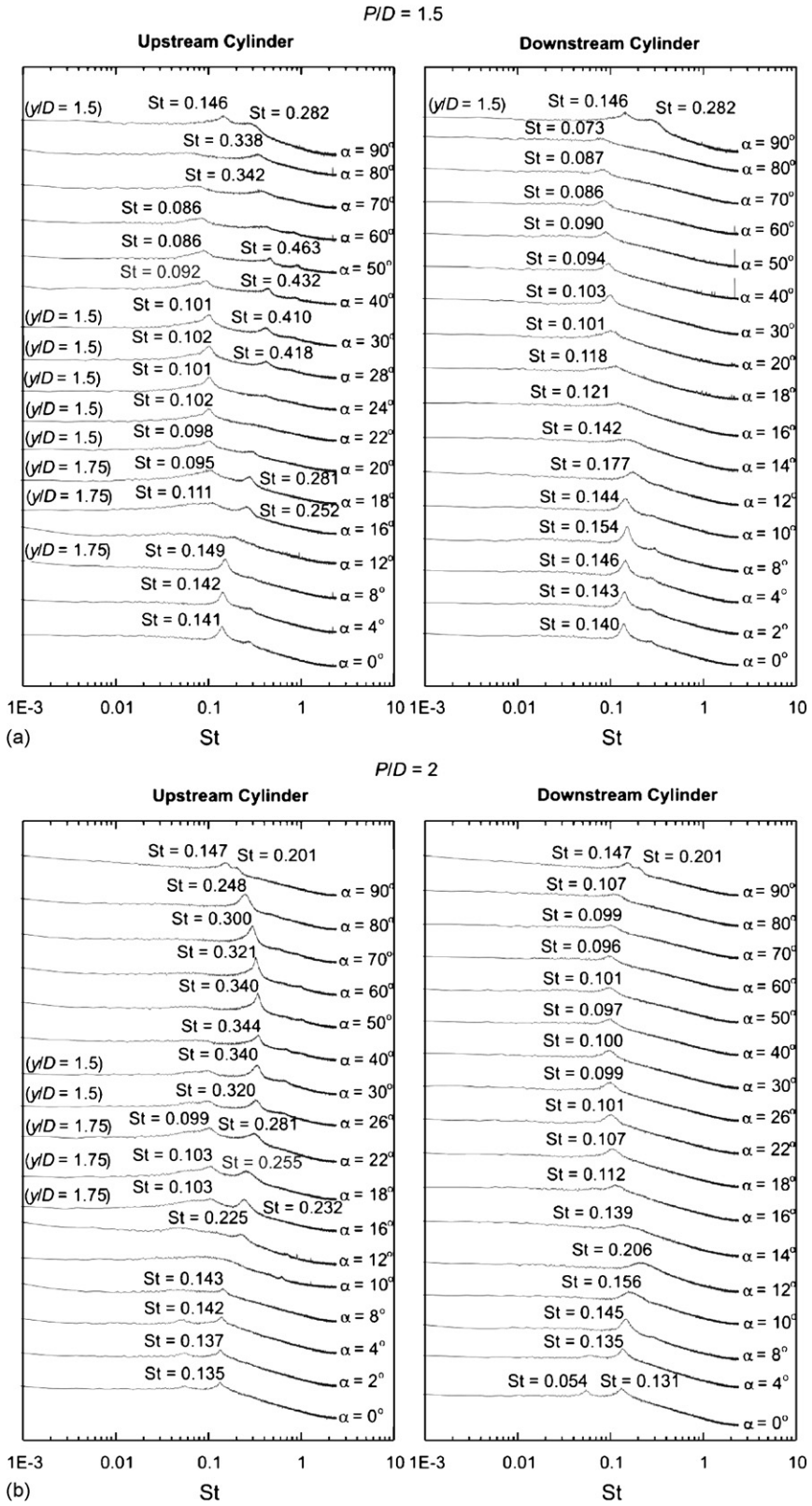

Fig. 9. Selected power spectra at mid-height ($z/H = 0.5$), as a function of incidence angle, for moderately spaced staggered finite circular cylinders: (a) $P/D = 1.5$; (b) $P/D = 2$; (c) $P/D = 2.5$; (d) $P/D = 3$. Each spectrum represents an average of 250 spectra. The vertical (logarithmic) scale of the graphs is arbitrary, but the same scale is used for each spectrum.

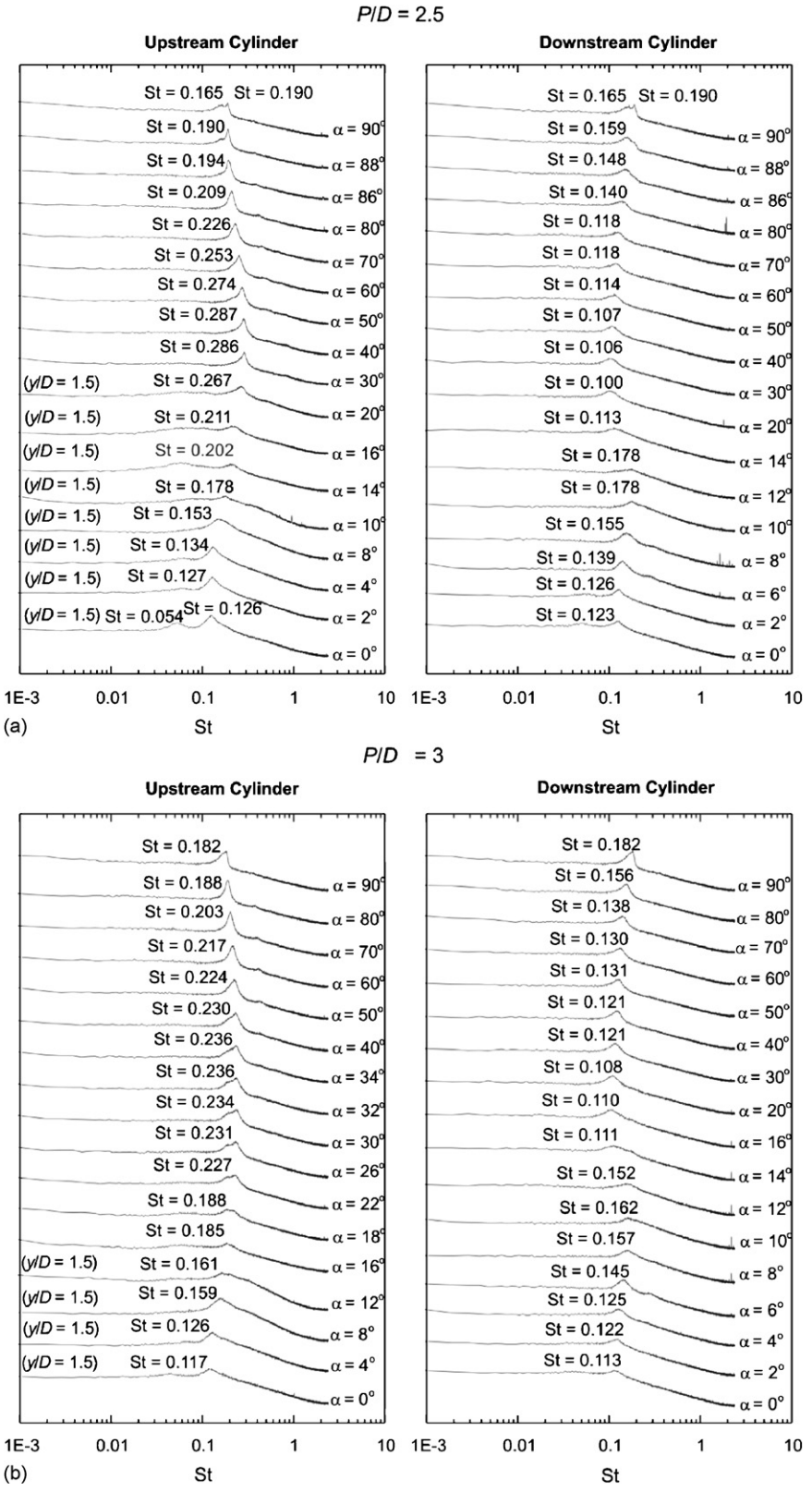

Fig. 9. (*Continued*)

upstream cylinder at incidence angles greater than the critical angle. Near the critical incidence angle, the peak in the power spectrum for the upstream cylinder either disappears or becomes very weak and broad-banded. When the cylinders are side-by-side, two peaks are measured for $P/D = 1.5$ (Fig. 9(a)), $P/D = 2$ (Fig. 9(b)) and $P/D = 2.5$ (Fig. 9(c)), which shows the existence of the bistable, biased flow pattern (where the flow is deflected, or biased, toward one of the two cylinders, typically in a bistable manner). As P/D increases, the two Strouhal numbers at $\alpha = 90^\circ$ become closer in value and change to a single St at $P/D = 3$ (Fig. 9(d)) with the disappearance of the biased flow pattern (Sumner et al., 1999).

4.1.3. *Widely spaced configurations ($P/D = 4, 5$)*

For widely spaced staggered configurations, the behaviour of the Strouhal number data (Fig. 10) at the mid-height position becomes less complex. There is no apparent critical incidence angle and generally the same Strouhal numbers are measured behind the upstream and downstream cylinders, except from $30^\circ < \alpha < 90^\circ$ for $P/D = 4$ (Fig. 10(a)) and from $45^\circ < \alpha < 82^\circ$ for $P/D = 5$ (Fig. 10(b)) where there are two distinct but adjacent St values. Over the range of α where two St numbers are measured, the higher St is associated with the vortex shedding from the upstream cylinder and the lower St is associated with vortex shedding from the downstream cylinder. Overall, the Strouhal numbers remain close to the value of a single finite circular cylinder ($St = 0.160$). The results indicate that there still exists some interference between the two cylinders, but the two cylinders behave more independently and shed vortices more like two single, isolated finite circular cylinders. This is similar to the behaviour of two widely spaced staggered infinite cylinders (Fig. 10(a)) (Sumner et al., 2005), where the vortex impingement (VI, where Kármán vortices shed from the upstream cylinder impinge upon the downstream cylinder) and the synchronized vortex shedding flow patterns are observed (Sumner et al., 2000).

It is noted that for $P/D = 3$ (Fig. 8(d)), two staggered *infinite* cylinders illustrate the widely spaced behaviour (Sumner et al., 2005) while the *finite* cylinders (at the mid-height position) still behave similar to moderately spaced cylinders. This difference is caused by the variation of the vortex formation length along the axis of the finite cylinder. Here, the Strouhal number of the finite cylinders is measured at the mid-height position, where the vortex formation length attains its maximum value and is longer than that of the infinite cylinder (Sumner et al., 2004). The two finite cylinders therefore have a longer interference region at mid-height, which delays the switchover from the moderately spaced behaviour to the widely spaced behaviour.

For the power spectra (Fig. 11), strong vortex shedding peaks are found behind both cylinders for most incidence angles. Weak vortex shedding peaks are found behind the downstream cylinder for the tandem ($\alpha = 0^\circ$) and nearly tandem ($\alpha = 4^\circ$) configurations, which can be attributed to the impingement of vortices shed from the upstream cylinder. For $P/D = 5$ (Fig. 11(b)), weak vortex shedding peaks are found behind the downstream cylinder at $\alpha = 12$–14°; this is similar to what was observed by Sumner et al. (2005) for two widely spaced *infinite* cylinders, and is

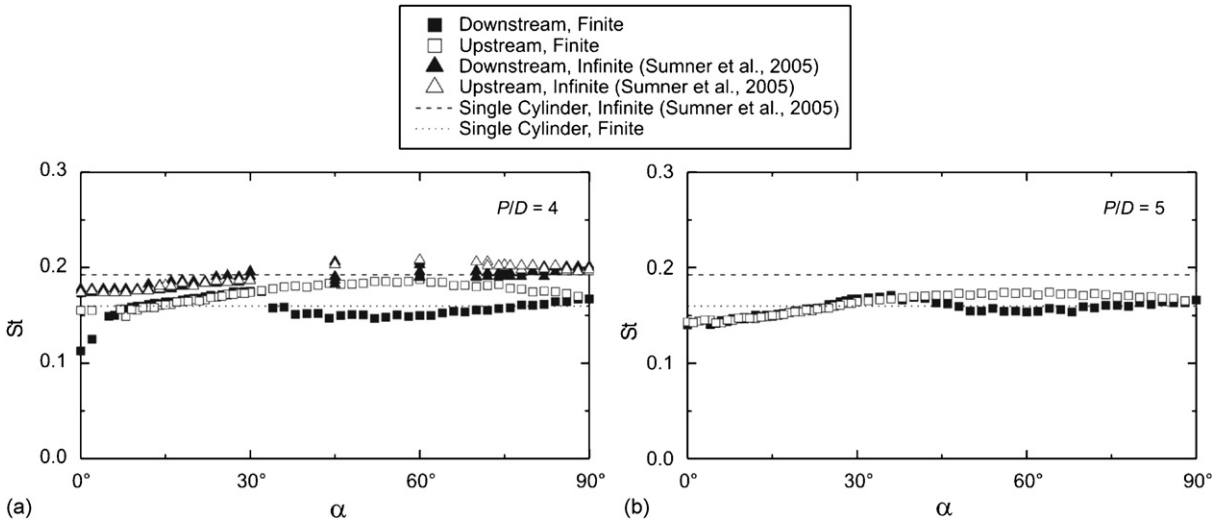

Fig. 10. Strouhal number data measured at mid-height ($z/H = 0.5$) for two widely spaced staggered finite circular cylinders: (a) $P/D = 4$; (b) $P/D = 5$. Symbols as in Fig. 6.

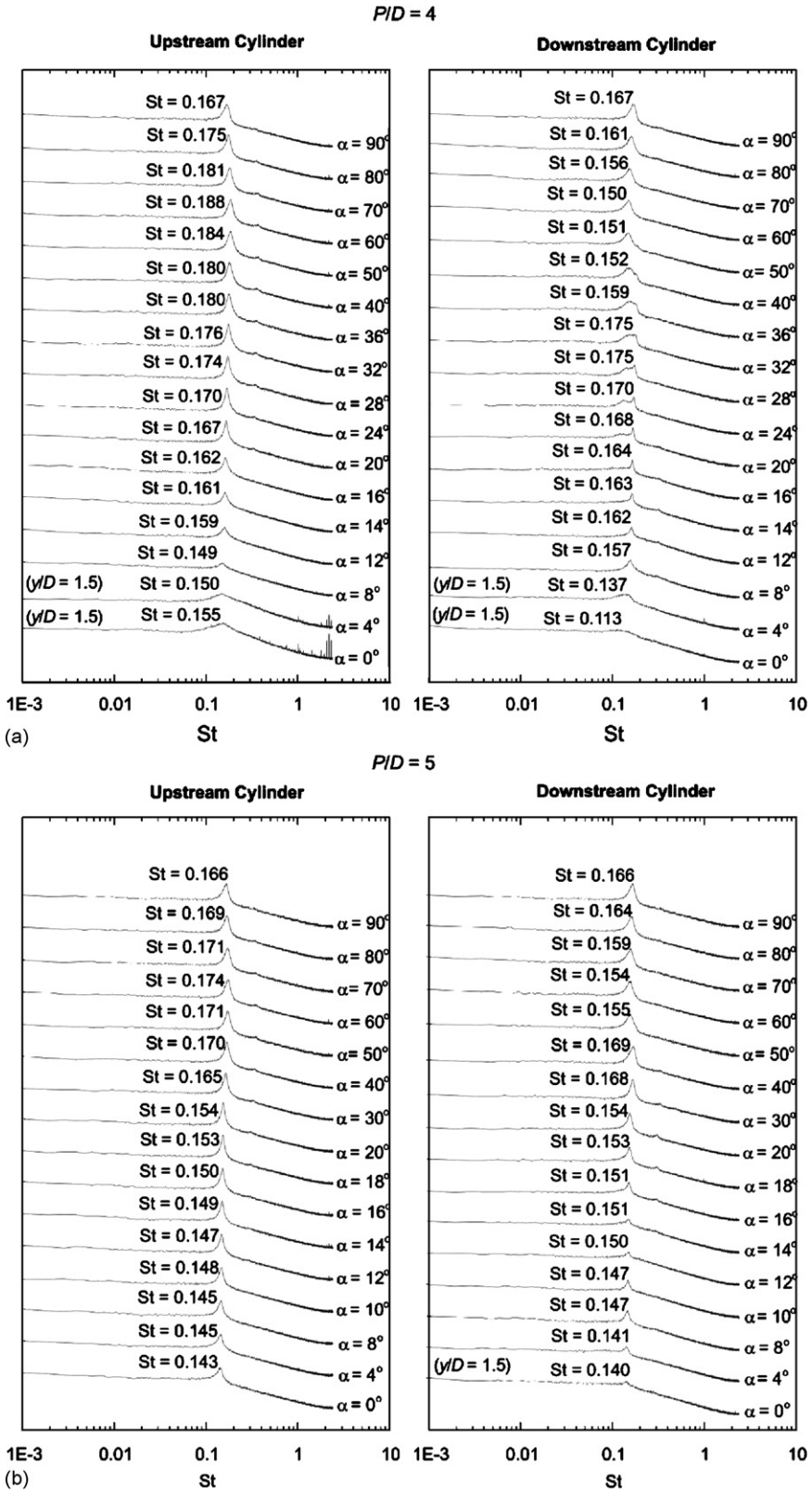

Fig. 11. Selected power spectra at mid-height ($z/H = 0.5$), as a function of incidence angle, for widely spaced staggered finite circular cylinders: (a) $P/D = 4$; (b) $P/D = 5$. Each spectrum represents an average of 250 spectra. The vertical (logarithmic) scale of the graphs is arbitrary, but the same scale is used for each spectrum.

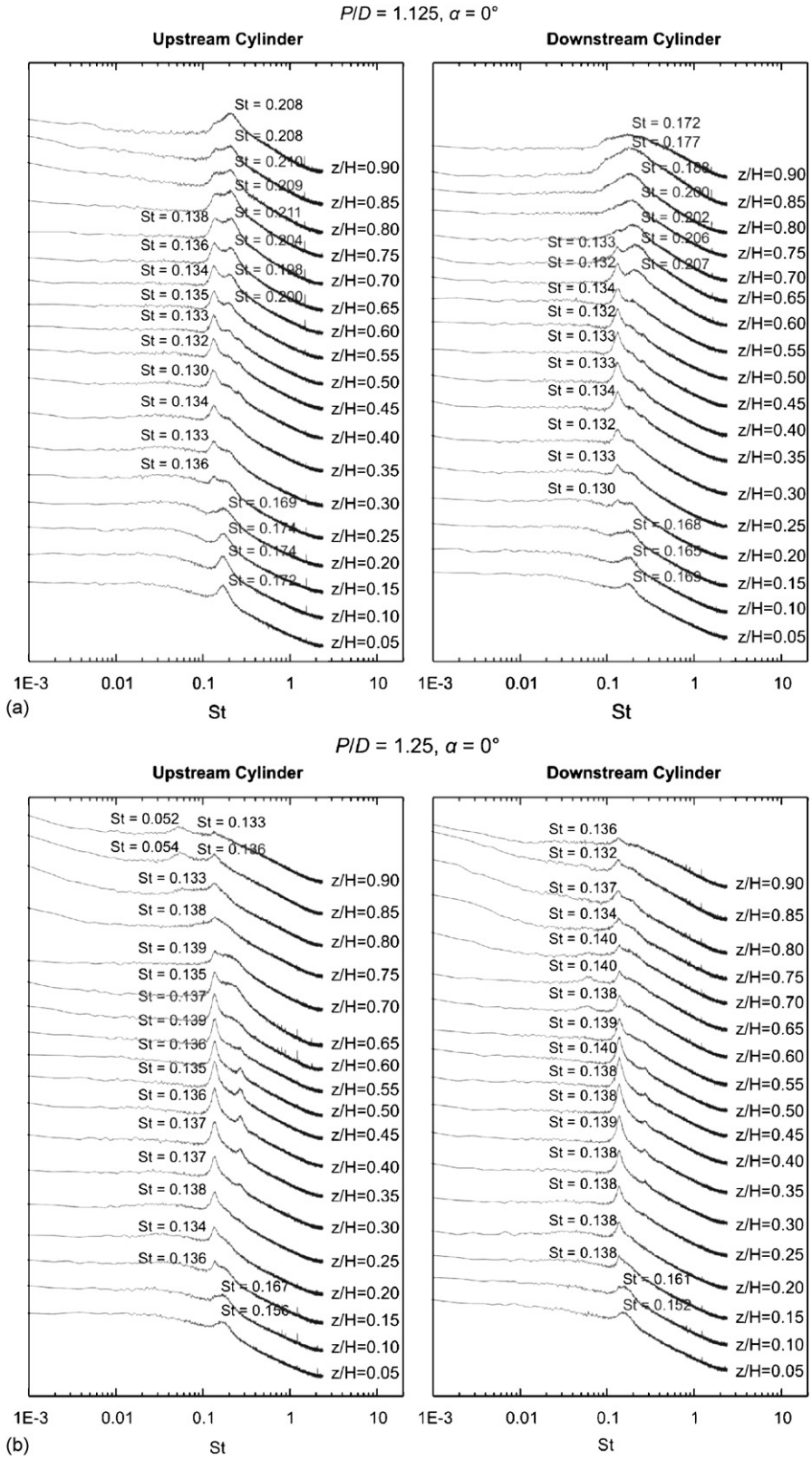

Fig. 12. Power spectra along the vertical lengths of the cylinders for closely spaced staggered configurations, where $\delta/H = 0.4$: (a) $P/D = 1.125$, $\alpha = 0^\circ$; (b) $P/D = 1.25$, $\alpha = 0^\circ$. Each spectrum represents an average of 250 spectra. The vertical (logarithmic) scale of the graphs is arbitrary, but the same scale is used for each spectrum.

the evidence of "outer lift peak",[2] where the mean lift coefficient on the downstream cylinder attains a local maximum value with incidence angle (Zdravkovich and Pridden, 1977; Sumner et al., 2005). The weakness of these peaks is less evident for $P/D = 4$ (Fig. 11(a)). A transitional-type behaviour can be seen in the downstream-cylinder power spectra for $P/D = 4$ (Fig. 11(a)), where there is a gradual changeover from a higher vortex shedding frequency to a lower vortex shedding frequency from $\alpha = 24^\circ$ to 50°; this may signal the change in flow pattern from VI to SVS.

4.2. Strouhal number measurements along the vertical lengths of the cylinders

Several experiments were conducted to investigate how the vortex shedding behaviour and Strouhal numbers change along the *vertical lengths* of the cylinders, from the ground plane to the free end (Figs. 12–18). These experiments were performed only for selected staggered configurations, i.e. for specific combinations of P/D and α representing closely spaced, moderately spaced, and widely spaced arrangements (as identified in Section 4.1).

4.2.1. Closely spaced configurations

The power spectra measured along the vertical lengths of the cylinders, for selected closely spaced staggered configurations, are shown in Figs. 12–14.

When the two closely spaced finite circular cylinders are arranged in tandem, at $P/D = 1.125$ and 1.25, the shape of power spectra varies considerably along the cylinders (Fig. 12). The general tendency is for the peaks to be weaker and more broad-banded near the base and the free end of the cylinders, similar to a single, isolated finite circular cylinder (Fig. 5), but there are also changes to the value of the Strouhal number along the cylinders. For $P/D = 1.125$ (Fig. 12(a)), the peaks of power spectra shift from a high vortex shedding frequency ($\mathrm{St} \approx 0.17$) near the base of the finite cylinder to a low vortex shedding frequency ($\mathrm{St} \approx 0.13$) around the mid-height of the cylinder, and finally change back to a higher (although broad-banded) vortex shedding frequency ($\mathrm{St} \approx 0.20$) near the free end. For $P/D = 1.25$ (Fig. 12(b)), the behaviour is different: the peaks of power spectra shift from $\mathrm{St} \approx 0.16$ to 0.14 at $z/H = 0.15$ and then remain the same up to the free end of the cylinder, with only the shape of the peak changing. The behaviour of the peaks and Strouhal number suggest that the flow pattern varies along the vertical axes of the cylinders (Luo et al., 1996). Here, it may be that the shear layers from the upstream cylinder wrap around the downstream cylinder for most of the vertical length, and roll-up into Kármán vortices behind the downstream cylinder. This shear layer behaviour becomes disturbed near the ground plane and near the free end, resulting in different local flow patterns and Strouhal numbers. It is noted that with the cylinders placed very close together, the "downwash" flow generated at the free end of upstream cylinder is blocked by the downstream cylinder and only part of the flow can travel down into the gap between the two cylinders, while the rest has to move over the downstream cylinder and then descend to the near-wake region.

For two closely spaced staggered cylinders at small incidence angles, such as at $\alpha = 30^\circ$ (Fig. 13), the behaviour of the power spectra along the vertical axes of the cylinders is less complex than for $\alpha = 0^\circ$ (Fig. 12). The peaks of the power spectra are weaker and more broad-banded near to the ground plane and close to the free end. The strongest peaks are seen near the mid-height position and for the downstream cylinder. For $P/D = 1.125$ and $\alpha = 30^\circ$ (Fig. 13(a)), the main vortex shedding peak (corresponding to $\mathrm{St} \approx 0.10$) becomes very weak or even disappears when $z/H \geqslant 0.6$; a similar behaviour is seen for $P/D = 1.25$ and $\alpha = 30^\circ$ (Fig. 13(b)). Near the free end, higher-frequency peaks appear in the power spectra.

When the two closely spaced cylinders are placed at large incidence angles (Fig. 14), the peaks of the power spectra are extremely weak along most of the cylinder, and in some cases the peaks are completely absent (Fig. 14(a), upstream cylinder). The strongest peaks are found near the mid-height position and for the downstream cylinder (Figs. 14(a) and (b)). For the side-by-side configuration (Figs. 14(c) and (d)), vortex shedding peaks are absent near the free end.

4.2.2. Moderately spaced configurations

The power spectra measured in the wall-normal direction along the cylinders, for selected moderately spaced staggered configurations, are shown in Figs. 15–17.

When the moderately spaced finite circular cylinders are arranged in tandem, strong vortex shedding peaks are seen along the vertical lengths of both cylinders (Fig. 15). The same Strouhal number is measured behind both the upstream and downstream cylinders. For $P/D = 2$ (Fig. 15(a)), when moving away from the ground plane, there is a transition at

[2]For two widely spaced staggered *infinite* circular cylinders, weakened vortex shedding peaks were found in the downstream-cylinder power spectra at the location of the "outer lift peak" (Sumner et al., 2005). For two staggered *finite* circular cylinders, force measurements would be needed to confirm the location of the outer lift peak (Zdravkovich and Pridden, 1977; Sumner et al., 2005).

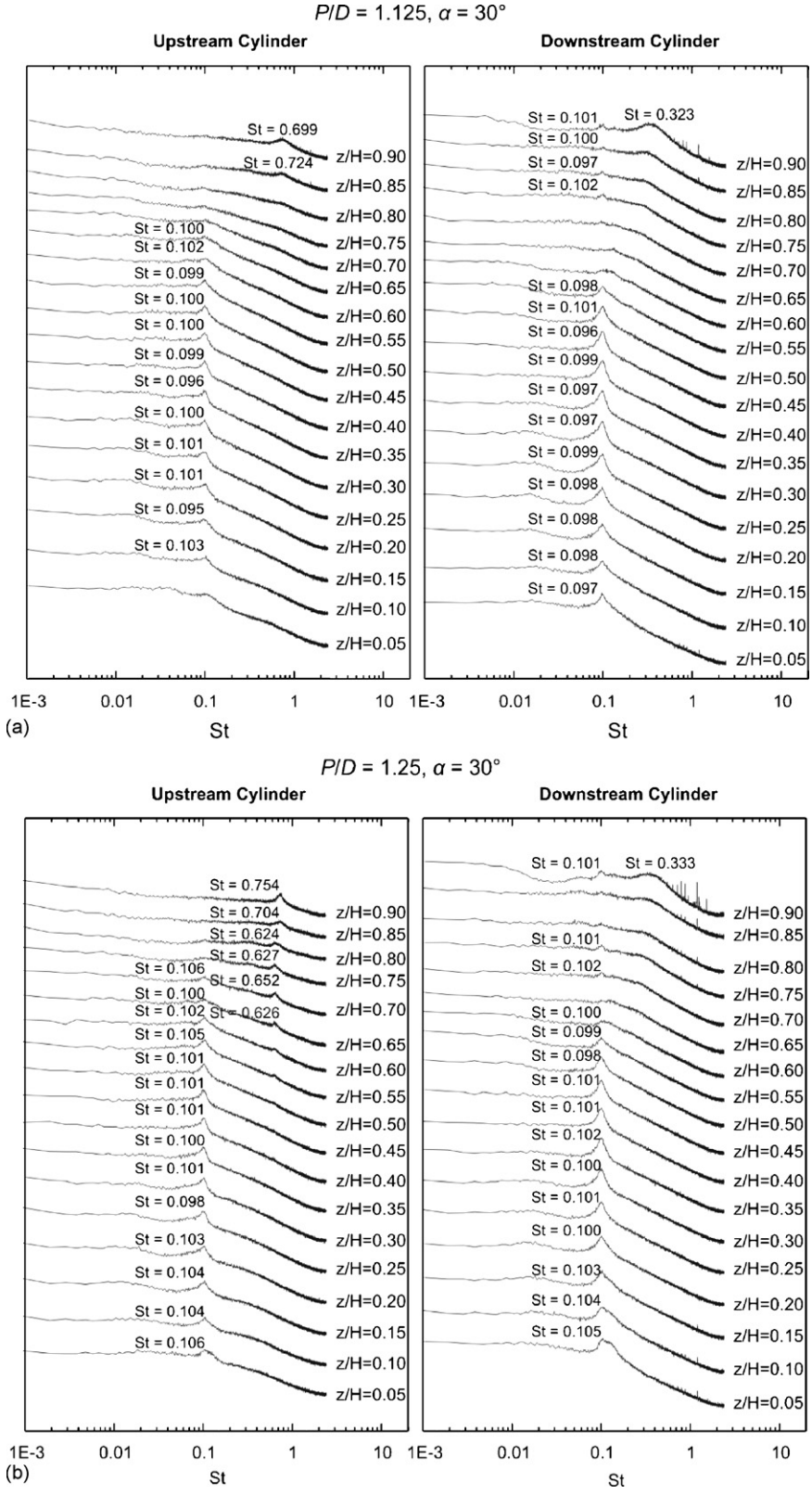

Fig. 13. Power spectra along the vertical lengths of the cylinders for closely spaced staggered configurations, where $\delta/H = 0.4$: (a) $P/D = 1.125$, $\alpha = 30^\circ$; (b) $P/D = 1.25$, $\alpha = 30^\circ$. Each spectrum represents an average of 250 spectra. The vertical (logarithmic) scale of the graphs is arbitrary, but the same scale is used for each spectrum.

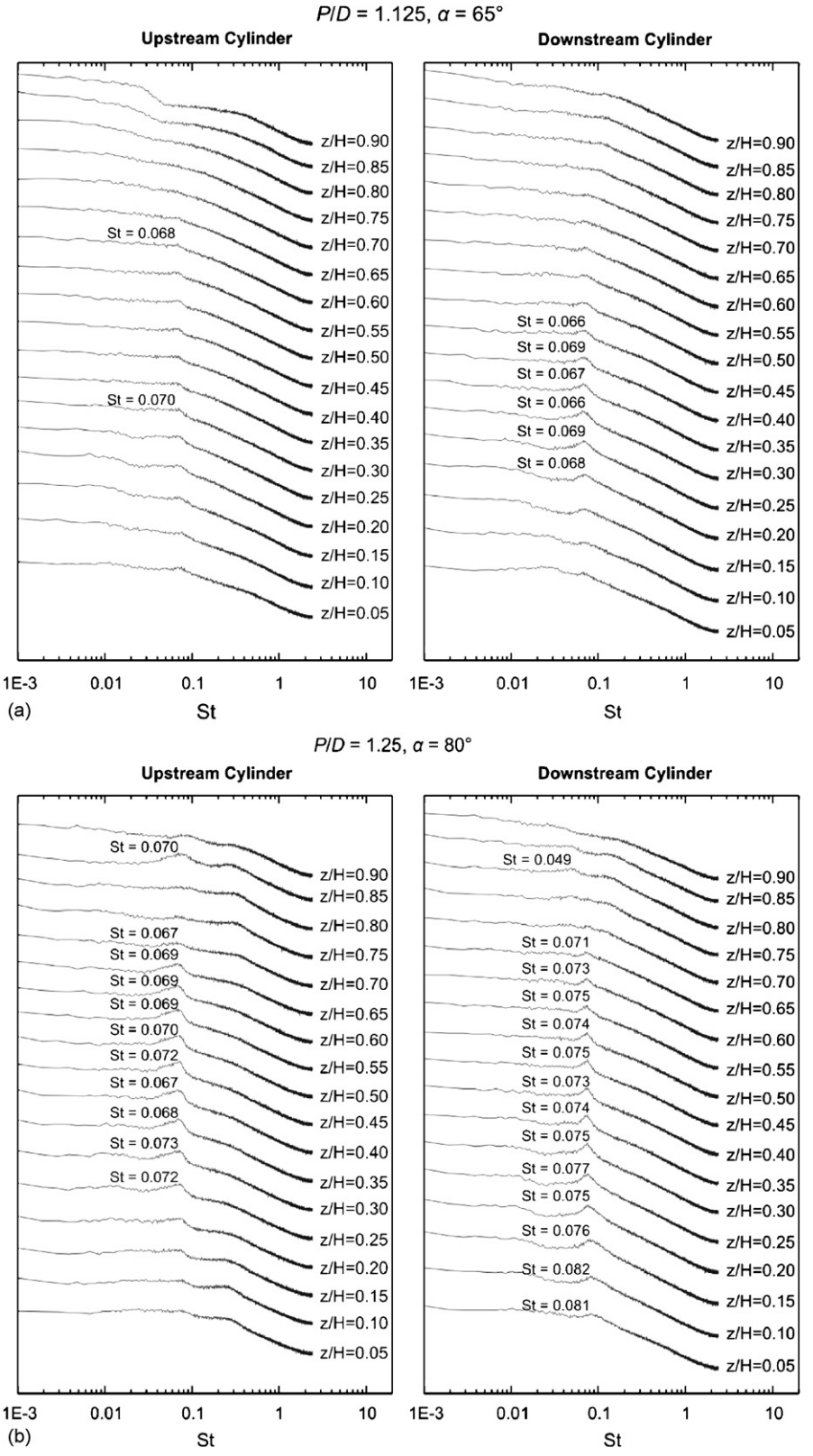

Fig. 14. Power spectra along the vertical lengths of the cylinders for closely spaced staggered configurations, where $\delta/H = 0.4$: (a) $P/D = 1.125$, $\alpha = 65^\circ$; (b) $P/D = 1.25$, $\alpha = 80^\circ$; (c) $P/D = 1.125$, $\alpha = 90^\circ$; (d) $P/D = 1.25$, $\alpha = 90^\circ$. Each spectrum represents an average of 250 spectra. The vertical (logarithmic) scale of the graphs is arbitrary, but the same scale is used for each spectrum.

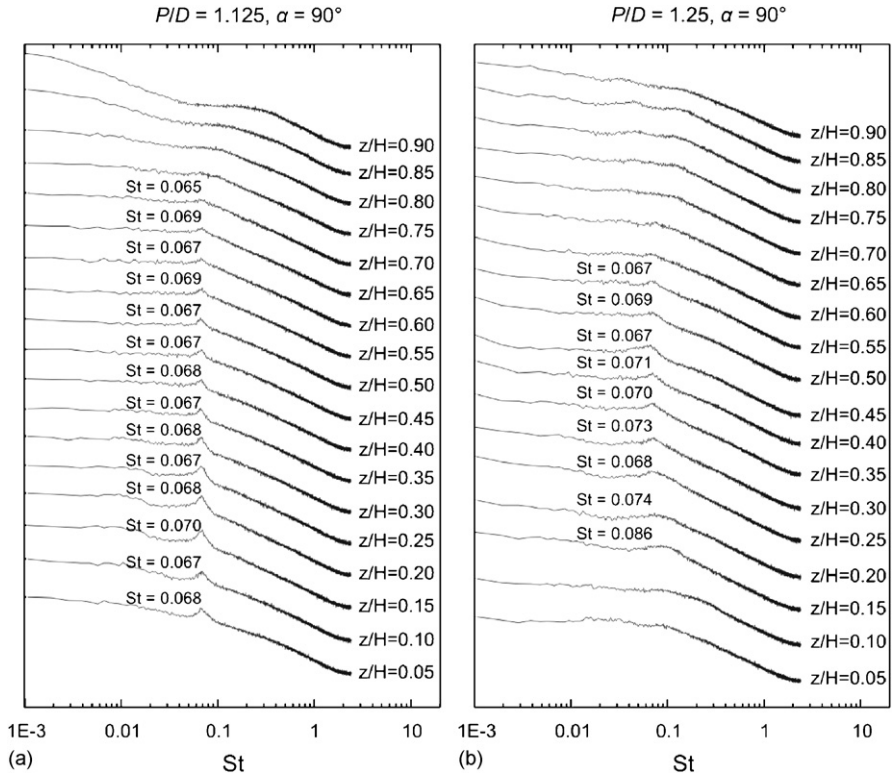

Fig. 14. (*Continued*)

$z/H \approx 0.5$ from a high Strouhal number ($St \approx 0.13$, for $z/H < 0.5$) to a low Strouhal number ($St \approx 0.055$, for $z/H > 0.6$); the high-frequency and low-frequency peaks co-exist in the power spectrum from $z/H = 0.5$ to 0.6. This behaviour of the peaks in the power spectra suggests that a change in flow pattern occurs near the mid-height of the two tandem cylinders (Luo et al., 1996). The high Strouhal number seen along most of the cylinders' vertical lengths would be associated with a shear layer reattachment flow pattern, where the shear layers from the upstream cylinder reattach onto the downstream cylinder, which is commonly observed for tandem infinite circular cylinders at $P/D = 2$ and 2.5. Close to the free end, however, the tip vortex structures and downwash interfere with the reattachment process, and a new flow pattern arises. The low value of the Strouhal number ($St \approx 0.055$) suggests that it may be associated with a tip vortex periodicity (compare with $St \approx 0.067$–0.076 for the single, isolated finite circular cylinder in Fig. 5). Similar behaviour is seen also for $P/D = 2.5$ (Fig. 15(b)), except that the transition from high frequency to low frequency (and the switch in flow pattern) takes place closer to the ground plane, with the first appearance of the lower Strouhal number occurring at $z/H = 0.35$. In addition, near the free end, a third, higher Strouhal number of $St \approx 0.166$ is detected in addition to the low value.

Looking at some intermediate staggered configurations, corresponding to $P/D = 2$, $\alpha = 60^\circ$ (Fig. 16(a)) and $P/D = 2.5$, $\alpha = 60^\circ$ (Fig. 16(b)), strong vortex shedding peaks are seen for the upstream cylinder, while weaker and more broad-banded peaks are seen for the downstream cylinder; the strongest vortex shedding peaks are found near the mid-height position. For $P/D = 2$, $\alpha = 60^\circ$ (Fig. 16(a)), the shape of the power spectrum and the value of the Strouhal number change along the vertical length of the upstream cylinder. Near the ground plane, for $z/H < 0.3$, the peak in the spectrum is wider and corresponds to a lower Strouhal number ($St \approx 0.237$). From $z/H = 0.25$–0.35 there is a switchover to a higher Strouhal number ($St \approx 0.323$); this higher Strouhal number persists until about $z/H = 0.65$. For $z/H > 0.65$, the spectra for the upstream cylinder are marked by a new pair of low and high Strouhal numbers. For the downstream cylinder, there is a gradual reduction in Strouhal number when moving away from the ground plane, and an absence of clearly defined vortex shedding peaks for $z/H > 0.65$. Similar variations in the power spectra are seen for $P/D = 2.5$, $\alpha = 60^\circ$ (Fig. 16(b)), although the values of the Strouhal numbers are different. The behaviour shown in Fig. 16 suggests there may be three distinct flow patterns along the vertical lengths of the cylinders, with the most complex flow occurring near the free end. Based on the understanding of the flow around two staggered infinite circular cylinders (Gu and Sun, 1999; Sumner et al., 2000, 2005), synchronized vortex shedding flow patterns would be expected.

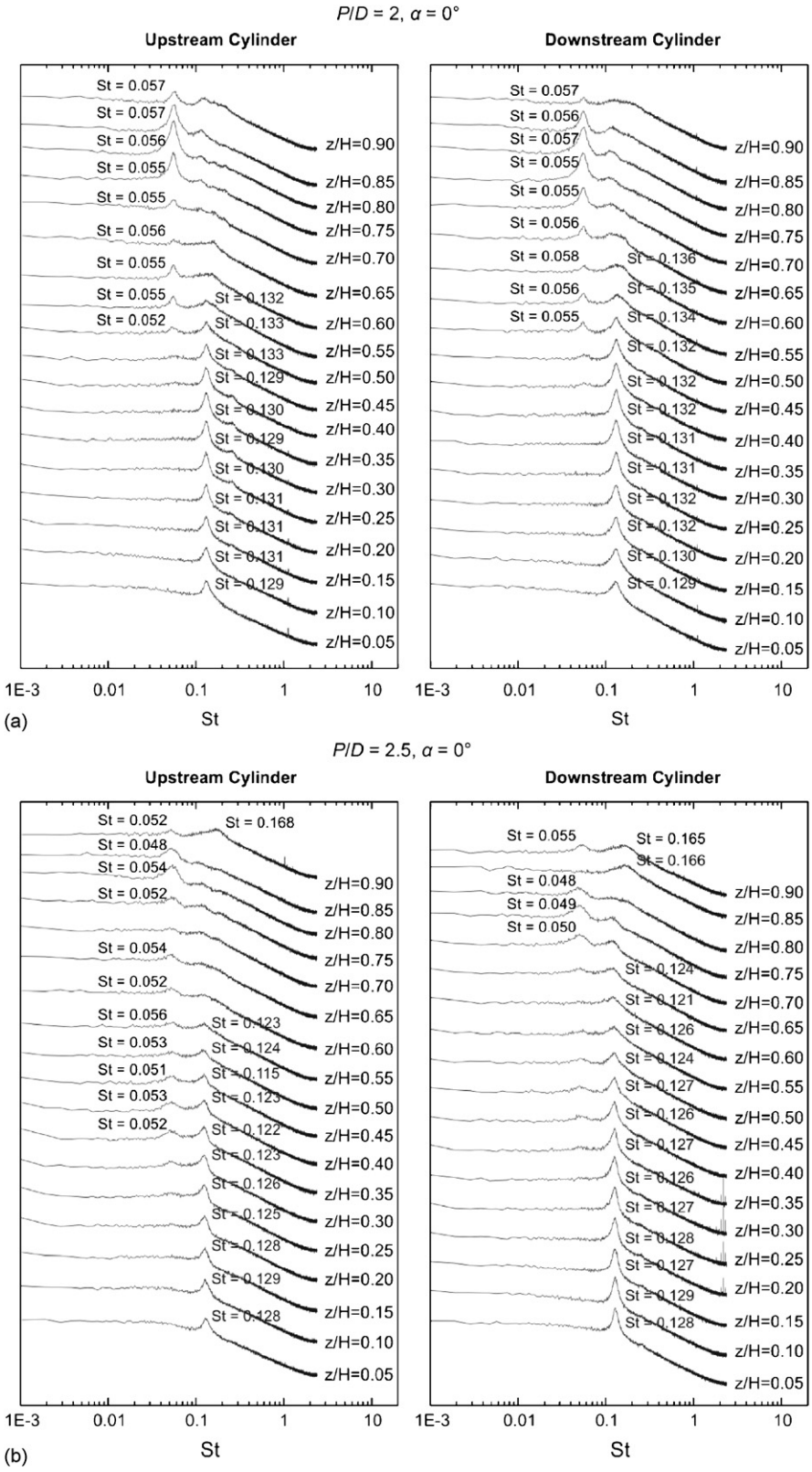

Fig. 15. Power spectra along the vertical lengths of the cylinders for moderately spaced staggered configurations, where $\delta/H = 0.4$: (a) $P/D = 2$, $\alpha = 0^{\circ}$; (b) $P/D = 2.5$ $\alpha = 0^{\circ}$. Each spectrum represents an average of 250 spectra. The vertical (logarithmic) scale of the graphs is arbitrary, but the same scale is used for each spectrum.

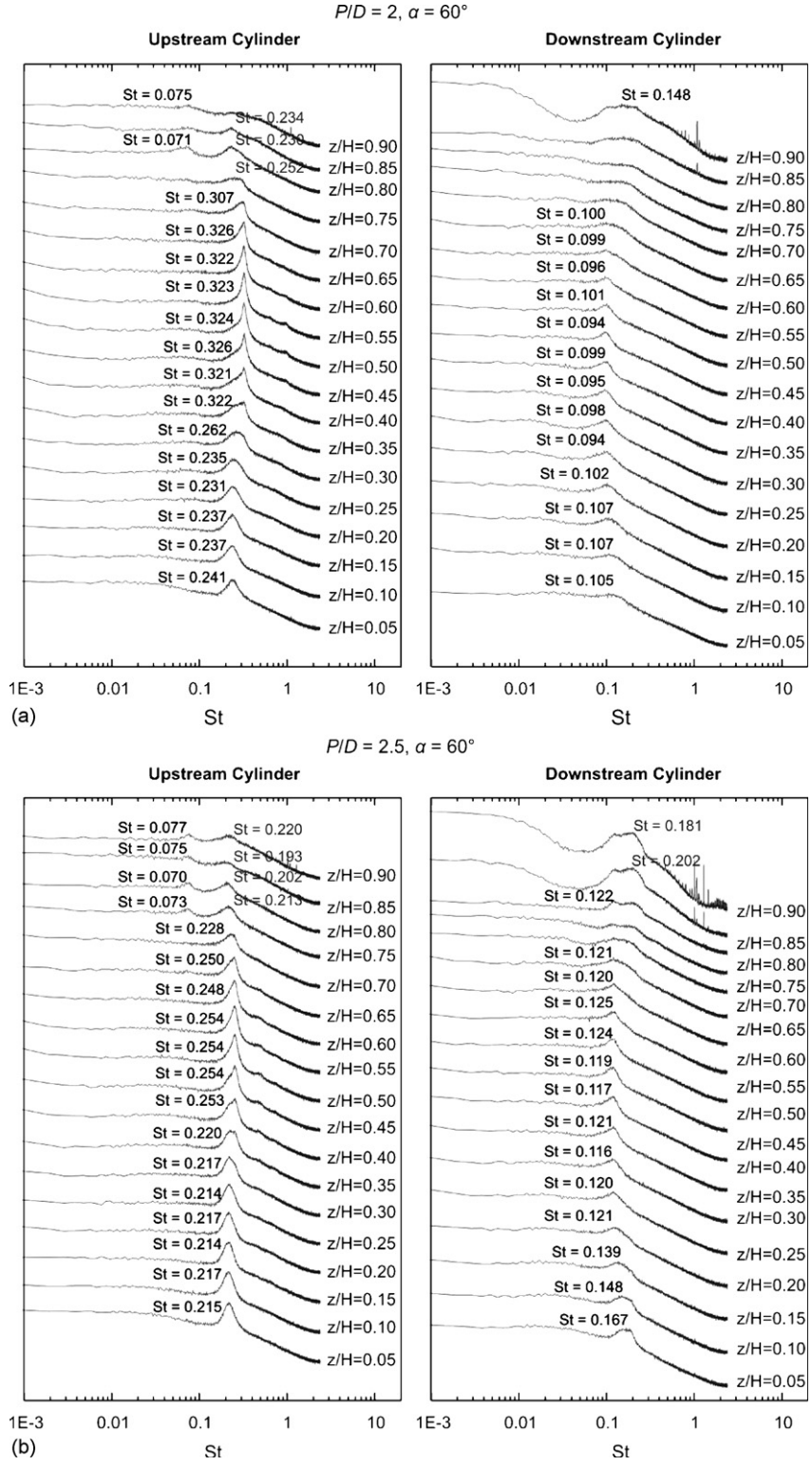

Fig. 16. Power spectra along the vertical lengths of the cylinders for moderately spaced staggered configurations, where $\delta/H = 0.4$: (a) $P/D = 2$, $\alpha = 60^\circ$; (b) $P/D = 2.5$ $\alpha = 60^\circ$. Each spectrum represents an average of 250 spectra. The vertical (logarithmic) scale of the graphs is arbitrary, but the same scale is used for each spectrum.

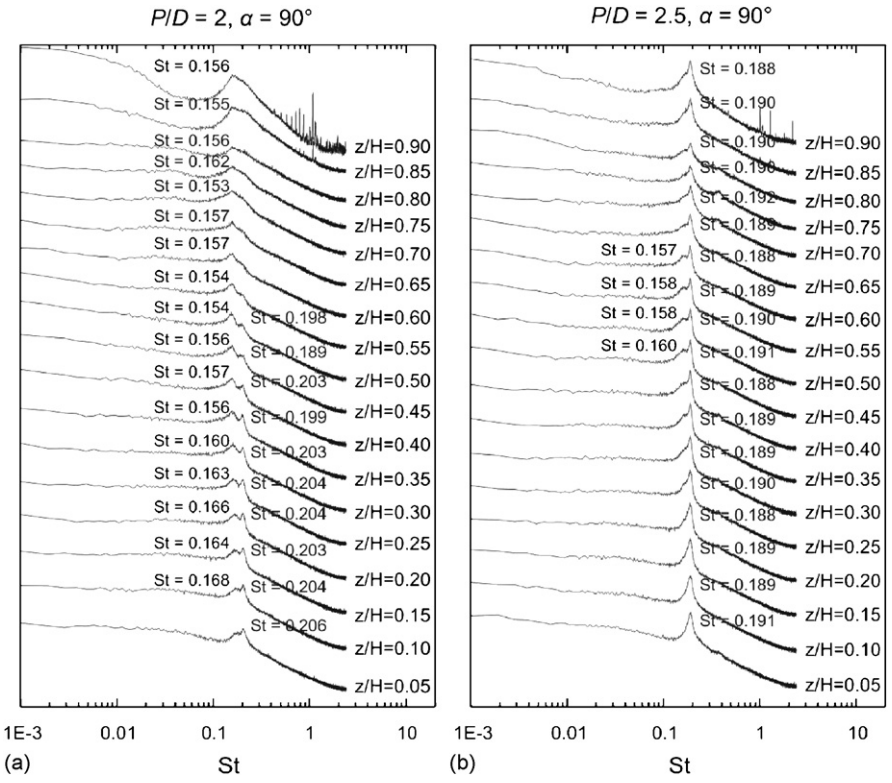

Fig. 17. Power spectra along the vertical lengths of the cylinders for moderately spaced staggered configurations, where $\delta/H = 0.4$: (a) $P/D = 2$, $\alpha = 90^\circ$; (b) $P/D = 2.5$ $\alpha = 90^\circ$. Each spectrum represents an average of 250 spectra. The vertical (logarithmic) scale of the graphs is arbitrary, but the same scale is used for each spectrum.

The changes in the Strouhal number along the vertical lengths of the cylinders could therefore be attributed to changes in the behaviour (strength, deflection angle) of the flow through the gap between the cylinders, as it is influenced by the flat-plate boundary layer on the ground plane or the separated flow from the free ends of the cylinders. Near the free end, the separated flow, downwash, and tip vortex structures disturb the regular Kármán vortex shedding processes from the cylinders, and the periodicity associated with the tip vortex structures is detected behind the upstream cylinder (St = 0.070–0.077).

In the side-by-side configuration, the power spectra for the finite circular cylinders (Fig. 17) show the existence of the bistable, biased flow pattern along parts of the cylinders, similar to what was reported by Zdravkovich (1980), Park and Lee (2003) and Liu and Cui (2006). For $P/D = 2$ (Fig. 17(a)), the power spectra for $z/H \leqslant 0.5$ show two vortex shedding peaks, the lower Strouhal number ($St \approx 0.153$–0.168) corresponding to vortex shedding from the cylinder with the wide near-wake region and the higher Strouhal number ($St \approx 0.195$–0.206) corresponding to vortex shedding from the cylinder with the narrow near-wake region. The values of these Strouhal numbers decrease slightly when moving away from the ground plane. For $z/H > 0.5$, there is only a single broad-banded peak corresponding to the lower value of the Strouhal number, suggesting the flow may be stably biased to one of the cylinders, perhaps due to the presence of the downwash from the free end. For $P/D = 2.5$ (Fig. 17(b)), two peaks are seen in the power spectra only for $z/H = 0.45$–0.6. The vortex shedding peaks are also stronger than the case of $P/D = 2$ (Fig. 17(a)).

4.2.3. *Widely spaced configurations*

For the widely spaced staggered configurations, experiments were performed along the vertical lengths of the cylinders for $P/D = 5$ only. Selected power spectra are shown in Fig. 18.

In the tandem configuration, the same Strouhal number ($St \approx 0.144$) is measured along the entire cylinder for both the upstream and downstream cylinders (Fig. 18(a)). This "co-shedding" flow pattern (Luo et al., 1996) is found along vertical lengths of the cylinders, where Kármán vortex shedding occurs from both cylinders at the same frequency. The strongest vortex shedding peaks are found for the upstream cylinder; although the peaks become weaker near the

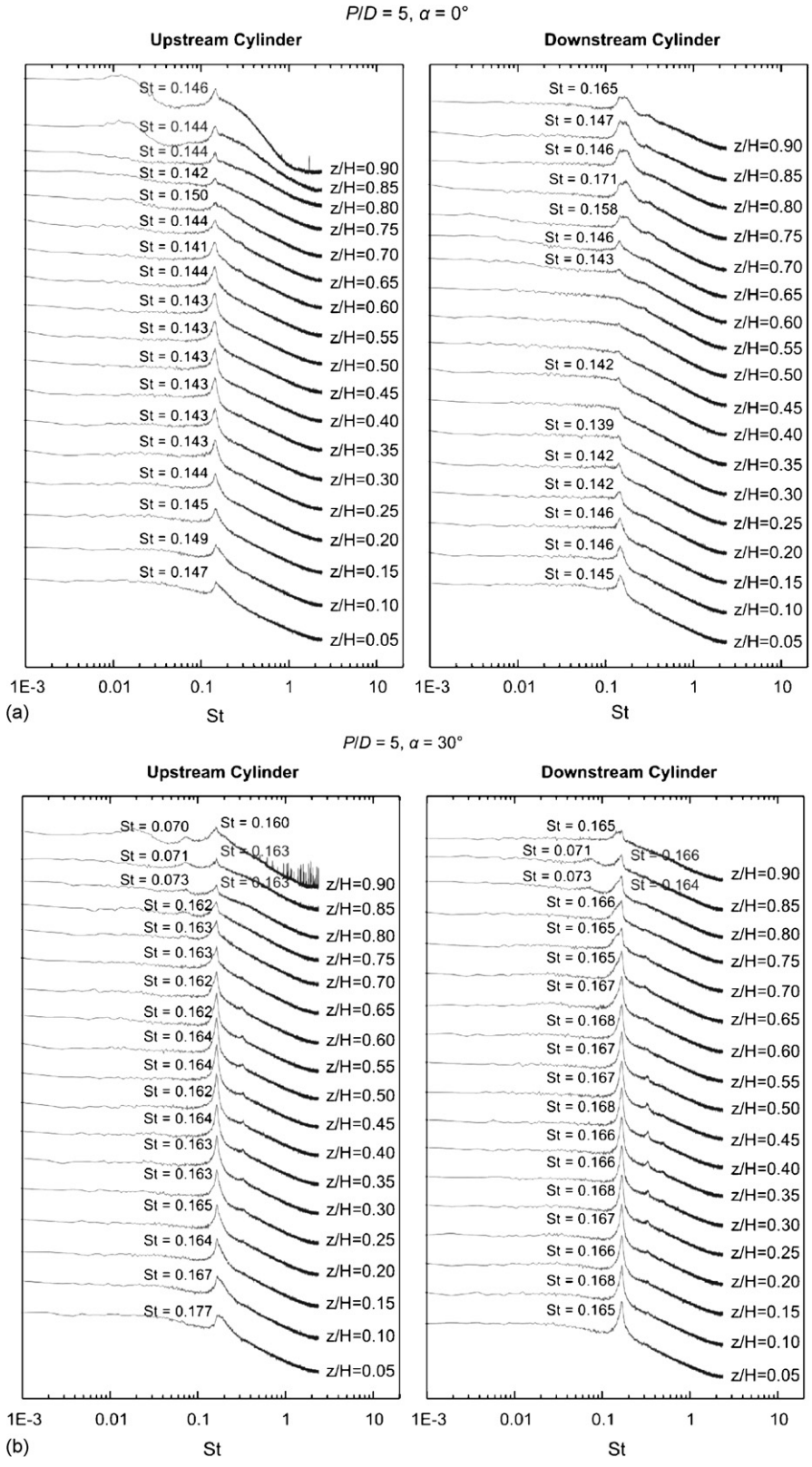

Fig. 18. Power spectra along the vertical lengths of the cylinders for widely spaced staggered configurations, where $\delta/H = 0.4$: (a) $P/D = 5$, $\alpha = 0^\circ$; (b) $P/D = 5$ $\alpha = 30^\circ$; (c) $P/D = 5$ $\alpha = 60^\circ$; (d) $P/D = 5$ $\alpha = 90^\circ$. Each spectrum represents an average of 250 spectra. The vertical (logarithmic) scale of the graphs is arbitrary, but the same scale is used for each spectrum.

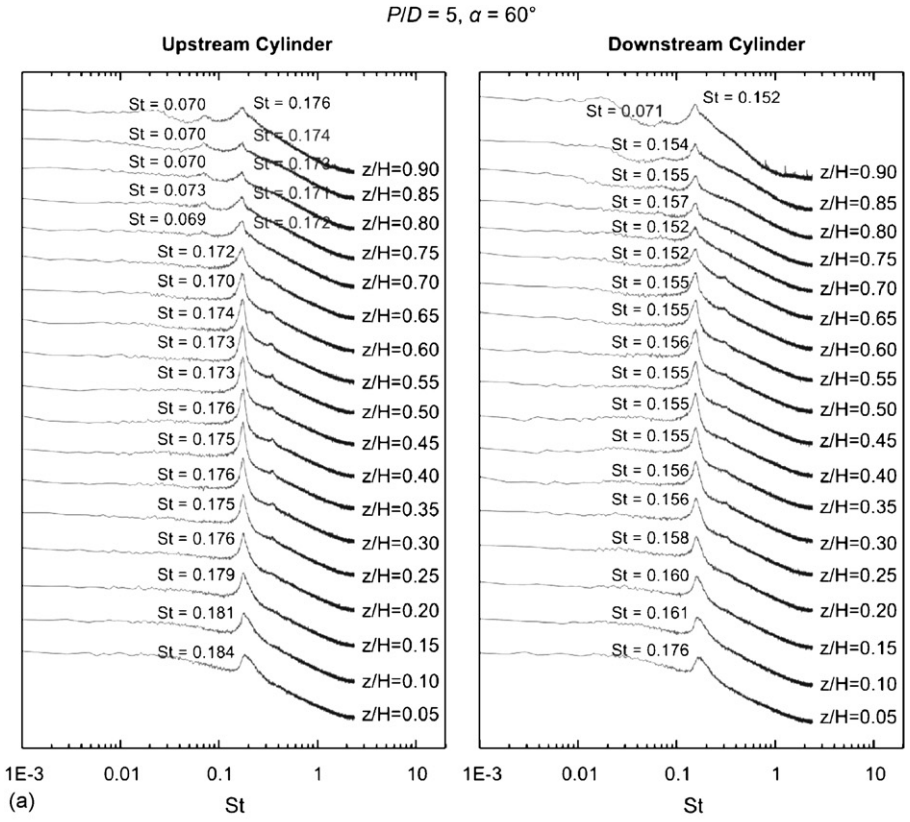

Fig. 18. (*Continued*)

free end, the shedding frequency is still detected up to $z/H = 0.9$ (Fig. 18(a)). For the downstream cylinder, the vortex shedding peaks are weaker compared to the upstream cylinder, with the peaks essentially absent from the spectra around the mid-height position. The weaker peaks for the downstream cylinder may be attributed to the impingement of Kármán vortices shed from the upstream cylinder (the VI flow pattern) (Sumner et al., 2000). Near the free end, for $z/H \geqslant 0.7$, the peaks become broad-banded and flat, suggesting there may be a second Strouhal number (note $St = 0.171$ for $z/H = 0.75$) in this region that is close in value to the primary Strouhal number. The low-frequency peaks associated with the periodicity of the tip vortex structures (Kitigawa et al., 2002) are not observed.

At intermediate angles of incidence of $\alpha = 30^\circ$ (Fig. 18(b)) and 60° (Fig. 18(c)), Kármán vortex shedding continues to occur from both cylinders, and a synchronized vortex shedding frequency flow pattern would be expected (Sumner et al., 2000). At $\alpha = 30^\circ$ (Fig. 18(b)), the same frequency is measured behind both cylinders, while at $\alpha = 60^\circ$ (Fig. 18(c)) the vortex shedding frequency of the downstream cylinder is slightly lower than that of the upstream cylinder. At both incidence angles, strong vortex shedding peaks are found along most of the vertical lengths of both the upstream and downstream cylinders. Weaker and more broad-banded peaks are found near the free ends and bases of the cylinders. Near the free end, for $z/H \geqslant 0.75$, a weak low-frequency peak of $St \approx 0.070$ is detected in the power spectra for both cylinders, which may be the periodicity associated with the tip vortex structures (Kitigawa et al., 2002).

When the cylinders are arranged side-by-side, strong vortex shedding peaks are found in the power spectra along mostly the entire vertical lengths of the cylinders (Fig. 18(d)). Similar to $\alpha = 30^\circ$ (Fig. 18(b)) and $\alpha = 60^\circ$ (Fig. 18(c)), very weak low-frequency peaks corresponding to $St \approx 0.070$ are detected near the free end, as in the case of the single, isolated finite cylinder (Fig. 5).

5. Conclusions

In the present study, vortex shedding from two staggered finite circular cylinders was studied experimentally in a low-speed wind tunnel at $Re_D = 2.4 \times 10^4$. Two identical finite-height circular cylinders of $AR = 9$ were used. The cylinders were mounted normal to a ground plane and were partially immersed in a turbulent flat-plate boundary layer, with $\delta/H = 0.4$ at the location of the cylinders. The cylinders were arranged in staggered configurations of $P/D = 1.125$, 1.25, 1.5, 2, 2.5, 3, 4 and 5, and incidence angles from $\alpha = 0^\circ$ to 90°. Hot-wire measurements were made behind both the upstream and downstream cylinders.

From measurements made at the mid-height position ($z/H = 0.5$), where the incidence angle was varied in small increments for each value of P/D, the Strouhal number behaviour could be broadly classified according to pitch ratio into closely spaced configurations ($P/D = 1.125$ and 1.25), moderately spaced configurations ($P/D = 1.5$, 2, 2.5 and 3) and widely spaced configurations ($P/D = 4$ and 5). This was similar to the case of two staggered infinite circular cylinders (Sumner et al., 2005), although a number of differences were highlighted. The results demonstrate the complex proximity interference and wake interference effects that can exist for groups of bluff bodies (such as chimneys, buildings, etc.) in cross-flow. Small changes in the incidence angle (wind direction) can lead to marked changes in the vortex shedding (dominant) frequencies, which may have implications when it comes to vortex-induced vibrations.

Measurements made along the vertical lengths of the cylinders, for selected closely spaced, moderately spaced, and widely spaced staggered configurations, showed that the vortex shedding peaks were weaker and more broad-banded near the base and the free end. For some closely spaced and moderately spaced configurations (particularly for cylinders in tandem and at small incidence angles), changes in the Strouhal number along the vertical lengths of the cylinders indicated that changes in the flow pattern had occurred. For a number of staggered configurations, up to four different Strouhal numbers may be found in the combined wake of the two cylinders. With changes in incidence angle (wind direction), the values of these Strouhal numbers may change and/or the number of dominant frequencies found in the wake may increase or reduce. These effects are attributed to the influence of proximity interference and wake interference on the flow patterns near the free ends of the cylinders, where the tip vortex structures and downwash flow fields develop and interact with Kármán vortex shedding and boundary layer separation.

Acknowledgments

The authors acknowledge the financial support of the Natural Sciences and Engineering Research Council of Canada (NSERC). The assistance of D.M. Deutscher and Engineering Shops is appreciated.

References

Adaramola, M.S., Akinlade, O.J., Sumner, D., Bergstrom, D.J., Schenstead, A.J., 2006. Turbulent wake of a finite circular cylinder of small aspect ratio. Journal of Fluids and Structures 22, 919–928.

Akbari, M.H., Price, S.J., 2005. Numerical investigation of flow patterns for staggered cylinder pairs in cross-flow. Journal of Fluids and Structures 20, 533–554.

Gu, Z.F., Sun, T.F., 1999. On interference between two circular cylinders in staggered arrangement at high subcritical Reynolds numbers. Journal of Wind Engineering and Industrial Aerodynamics 80, 287–309.

Kareem, A., Kijewski, T., Lu, P.C., 1998. Investigation of interference effects for a group of finite cylinders. Journal of Wind Engineering and Industrial Aerodynamics 77–78, 503–520.

Kitigawa, T., Fujino, Y., Kimura, K., Mizuno, Y., 2002. Wind pressures measurement on end-cell-induced vibration of a cantilevered circular cylinder. Journal of Wind Engineering and Industrial Aerodynamics 90, 395–405.

Kiya, M., Arie, M., Tamura, H., Mori, H., 1980. Vortex shedding from two circular cylinders in staggered arrangement. ASME Journal of Fluids Engineering 102, 166–173.

Krönke, I., Sockel, H., 2007. Measurement of extreme aerodynamic interference forces acting on circular cylinders in turbulent boundary layers. Journal of Wind Engineering and Industrial Aerodynamics 95, 1229–1241.

Liu, Y., Cui, Z.X., 2006. Two side-by-side cantilevered cylinders in a cross flow. In: Proceedings of PVP2006-ICPVT-11, 2006 ASME Pressure Vessels and Piping Division Conference, July 23–27, 2006, Vancouver, Canada, Paper No. PVP2006-ICPVT-11-93894, 9pp.

Luo, S.C., Gan, T.L., Chew, Y.T., 1996. Uniform flow past one (or two in tandem) finite length circular cylinders. Journal of Wind Engineering and Industrial Aerodynamics 59, 69–93.

Okamoto, S., Sunabashiri, Y., 1992. Vortex shedding from a circular cylinder of finite length placed on a ground plane. ASME Journal of Fluids Engineering 144, 512–521.

Palau-Salvador, G., Stoesser, T., Frohlich, J., Rodi, W., 2007. LES of the flow around two cylinders in tandem. In: Proceedings of the IUTAM Symposium on Unsteady Separated Flows and their Control, Corfu, Greece, June 18–22, 2007, 10pp.

Park, C.W., Lee, S.J., 2000. Free end effects on the near wake flow structure behind a finite circular cylinder. Journal of Wind Engineering and Industrial Aerodynamics 88, 231–246.

Park, C.W., Lee, S.J., 2003. Flow structure around two finite circular cylinders located in an atmospheric boundary layer: side-by-side arrangement. Journal of Fluids and Structures 17, 1043–1058.

Rooney, D.M., Rodichok, J., Dolan, K., 1995. Finite aspect ratio effects on vortex shedding behind two cylinder at angles of incidence. ASME Journal of Fluids Engineering 117, 219–226.

Sakamoto, H., Arie, M., 1983. Vortex shedding from a rectangular prism and a circular cylinder placed vertically in a turbulent boundary layer. Journal of Fluid Mechanics 126, 147–165.

Sakamoto, H., Oiwake, S., 1984. Fluctuating forces on a rectangular prism and a circular cylinder placed vertically in a turbulent boundary layer. ASME Journal of Fluids Engineering 106, 160–166.

Sarode, R.S., Gai, S.L., Ramesh, C.K., 1981. Flow around circular- and square-section models of finite height in a turbulent shear flow. Journal of Wind Engineering and Industrial Aerodynamics 8, 223–230.

Sumner, D., Richards, M.D., 2003. Some vortex-shedding characteristics of the staggered configuration of circular cylinders. Journal of Fluids and Structures 17, 345–350.

Sumner, D., Price, S.J., Païdoussis, M.P., 2000. Flow-pattern identification for two staggered circular cylinders in cross-flow. Journal of Fluid Mechanics 411, 263–303.

Sumner, D., Heseltine, J.L., Dansereau, O.J.P., 2004. Wake structure of a finite circular cylinder of small aspect ratio. Experiments in Fluids 37, 720–730.

Sumner, D., Richards, M.D., Akosile, O.O., 2005. Two staggered circular cylinders of equal diameter in cross-flow. Journal of Fluids and Structures 20, 255–276.

Sumner, D., Wong, S.S.T., Price, S.J., Païdoussis, M.P., 1999. Fluid behaviour of side-by-side circular cylinders in steady cross-flow. Journal of Fluids and Structures 13, 309–338.

Tanaka, S., Murata, S., 1999. An investigation of the wake structure and aerodynamic characteristics of a finite circular cylinder. JSME International Journal Series B: Fluids and Thermal Engineering 42, 178–187.

Taniguchi, S., Sakamoto, H., Arie, M., 1981. Flow around circular cylinders of finite height placed vertically in turbulent boundary layers. Bulletin of the JSME 24, 37–44.

Taniguchi, S., Sakamoto, H., Arie, M., 1982. Interference between two circular cylinders of finite height vertically immersed in a turbulent boundary layer. ASME Journal of Fluids Engineering 104, 529–536.

Uematsu, Y., Yamada, M., Ishii, K., 1990. Some effects of free-stream turbulence on the flow past a cantilevered circular cylinder. Journal of Wind Engineering and Industrial Aerodynamics 33, 43–52.

Zdravkovich, M.M., 1980. Aerodynamics of two parallel circular cylinders of finite height at simulated high Reynolds numbers. Journal of Wind Engineering and Industrial Aerodynamics 6, 59–71.

Zdravkovich, M.M., Pridden, D.L., 1977. Interference between two circular cylinders, series of unexpected discontinuities. Journal of Industrial Aerodynamics 2, 255–270.